MARMARA UNIVERSITY
INSTITUTE FOR GRADUATE STUDIES
IN PURE AND APPLIED SCIENCES

OPTIMIZATION OF SINTERING PARAMETERS AND POST-SINTERING CHARACTERIZATION IN MULLITE-ZIRCON CERAMICS

ELIF BAL

MASTER THESIS

Department of Metallurgical and Materials Engineering

Thesis Supervisor
Prof. Dr. Recep Artır

Thesis Co-Supervisor

Asst. Prof. Dr. Görkem Yumuşak

ISTANBUL, 2023

MARMARA UNIVERSITY
INSTITUTE FOR GRADUATE STUDIES
IN PURE AND APPLIED SCIENCES

OPTIMIZATION OF SINTERING PARAMETERS AND POST-SINTERING CHARACTERIZATION IN MULLITE-ZIRCON CERAMICS

ELIF BAL
524719002

MASTER THESIS

Department of Metallurgical and Materials Engineering

Thesis Supervisor
Prof. Dr. Recep Artır

Thesis Co-Supervisor

Asst. Prof. Dr. Görkem Yumuşak

ISTANBUL, 2023

M A R M A R A U N I V E R S I T Y
INSTITUTE FOR GRADUATE STUDIES IN PURE AND APPLIED SCIENCES

Elif BAL, a Master of Science student of Marmara University, Institute for Graduate Studies in Pure and Applied Sciences, defended her thesis entitled "Optimization of sintering parameters and post sintering characterization in mullite-zircon ceramics", on …….. and has been foundto be satisfactory by the jury members.

Jury Members

Prof.Dr. Recep ARTIR (Advisor)
Marmara University .....(SIGN) .....

Assoc.Prof.Dr. Seval GENÇ (Jury Member)
Marmara University.....(SIGN) .....

Assoc.Prof.Dr.Ahmet TURAN (Jury Member)
Yeditepe University .....(SIGN) .....

A P P R O V A L

Marmara University Institute for Graduate Studies in Pure and Applied Sciences Executive Committee approves that Elif BAL be granted the degree of Master of Science in Metallurgical and Materials Program, on ……..……. (Resolution no: …...…….).

Director of the Institute
Prof. Dr. Bülent EKİCİ

ACKNOWLEDGEMENT

I would like to acknowledge and give my warmest thanks to my supervisors Prof. Dr. Recep Artır and Asst. Prof. Dr. Görkem Yumuşak who supported me in this work. I would also like to thank Parsan Steel forging and Machining Co., for making this work possible with their support. I would also like to give special thanks to my family and my friends for their continuous support and understanding.

January/2023 **Elif BAL**

TABLE OF CONTENTS

ACKNOWLEDGEMENT i
TABLE OF CONTENTS ii
ÖZET iv
ABSTRACT v
SYMBOLS vi
ABBREVIATIONS viii
LIST OF FIGURES ix
LIST OF TABLES xi
1. INTRODUCTION 1
1.1. Definition of Ceramics 1
1.2. Ceramic Matrix Composites 2
1.3. Mullite 3
1.4. Zircon 6
1.5. Mullite-Zircon Composites 9
1.6. Liquid-Phase Sintering of Ceramics 9
1.7. The Aims of the Project 10
2. LITERATURE SURVEY 11
2.1. The Synthesis of Mullite/Zirconia Composite Materials Doped With Boron Minerals. 11
2.2. Effect of Yttria on Mechanical and Microstructural Properties of Reaction Sintered Mullite-Zirconia Composites 11
2.3. Effects of Fe_2O_3 Concentration on Microstructures and Properties of SiC-based Ceramic Foams 12
2.4. Low-Temperature Co-Sintering for Fabrication of Zirconia/Ceria Bi-Layer Electrolyte via Tape Casting Using a Fe_2O_3 Sintering Aid 13
3. EXPERIMENTAL STUDIES 14
3.1. Raw Materials 14
3.1.1. Mullite-Zircon 14
3.1.2. Binder 14
3.1.3. Iron Oxide 14
3.2. Preparation of Powders 15
3.3. Compaction of the Powder Mixture 16

3.4. Sintering 17
3.5. Characterization of Samples 19
3.5.1. Sample preparation for ceramography and hardness test 19
3.5.2. XRD analysis of powders 20
3.5.3. Density and porosity and shrinkage measurements 22
3.5.4. Hardness test 24
3.5.5. Microstructural analysis 27
4. RESULTS AND DISCUSSIONS 28
4.1. XRD Results 28
4.2. Density 33
4.3. Porosity 34
4.4. Hardness 36
4.5. Surface Area Shrinkage 37
4.6. Water Absorption 37
4.7. Microstructure Evaluation 39
5. CONCLUSIONS 41
6. REFERENCES 42
BIOGRAPHY 45

ÖZET

MÜLLİT-ZİRKON SERAMİKLERİNDE SİNTERLEME PARAMETRELERİNİN OPTİMİZASYONU VE SİNTERLEME SONRASI KARAKTERİZASYONU

Müllit-zirkon sistemi yüksek sinterleme sıcaklıklarına (1500-1550 °C) sahip refrakter bir karışımdır. Bu çalışmada, sinterleme yardımcı katkı maddesi ilave edilerek sıvı faz sinterleme yöntemi kullanılarak uygun maliyetli işleme koşullarına sahip sinterleme sıcaklığını düşürmek için optimum parametrelerin belirlenmesi amaçlanmıştır. Sinterleme yardımcısı olarak Fe2O3, Mullite-Zirkon karışımına ağırlıkça %1, ağırlıkça %2 ve ağırlıkça %3 aralığında karıştırılmış ve bağlayıcı olarak da ağırlıkça %1 PAN kullanılmıştır. Bu karışım, 17.2369 MPa'lık (2500 psi) seçilen presleme kuvveti altında sinterlemeden önce topak haline getirildi. Bu peletler sırasıyla 1400°C, 1450°C ve 1500°C sinterleme sıcaklıklarında, her sıcaklık için 5 saatlik bir sinterleme süresi ile sinterlenmiştir.

Sıvı faz sinterleme işlemleri sonucunda mullit-zirkon sistemi için karakterizasyon yöntemleri kullanılarak sinterleme sıcaklığının etkisi ve sinterleme yardımcı katkı miktarının etkisi belirlenmiştir. 1400°C, 1450°C ve 1500°C sinterleme sıcaklıkları için gözeneklilik, sertlik, yoğunluk, su emme, büzülme ölçümleri ve mikroyapı ve XRD analizleri dahil olmak üzere sinterleme yardımcısı katkılı ve katkısız sinterlenmiş numunelerin bazı özellikleri.

Genel olarak sıcaklık arttıkça porozitenin azaldığı ve sıkılaşmanın iyileştiği gözlenmiştir. Berrak bir reaksiyon ürünü veya bağ tespit edilmedi ve demir oksit ile Mullit –Zirkon karışımı arasında bir faz oluştu. 1450°C ve 1500°C sıcaklıklar için ağırlıkça %2 ve ağırlıkça %3 oranında demir oksit ilavesi ile sertlik değerlerinde artış gözlenmiştir. Numuneye ağırlıkça %1 oranında demir oksit ilavesi, malzemenin sertliğini olumsuz yönde etkiler. Sinterleme yardımcı katkı maddesi demir oksit, yoğunluk üzerinde en iyi pozitif etkiyi 1450°C'de ağırlıkça %1 - ağırlıkça %2 ilavesi için sağlar, ancak daha yüksek ilave, mullit-zirkon karışımı üzerinde olumsuz bir etkiye sahip olabilir.

Sonuç olarak, sinterleme sıcaklığındaki artışın ve Mullit-Zirkon karışımına Fe_2O_3 sinterleme yardımcısı ilavesinin sinterlemeyi teşvik ettiği ve poroziteyi azalttığı bulunmuştur. Bu sonuçlar, Fe_2O_3 ilavesinin mikroyapının yoğunlaştırılması, fiziksel ve mekanik özelliklerin iyileştirilmesi üzerinde olumlu bir etkiye sahip olduğunu göstermektedir.

ABSTRACT

OPTIMIZATION OF SINTERING PARAMETERS AND POST-SINTERING CHARACTERISATION IN MULLITE-ZIRCON CERAMICS

The mullite-zircon system is a refractory mixture with high (1500-1550 °C) sintering temperatures. In this study, it is aimed to determine the optimum parameters to reduce the sintering temperature by adding a sintering aid additive and using the liquid phase sintering method to have cost effective processing conditions. As a sintering aid additive Fe_2O_3 was mixed into the Mullite-Zircon mixture in the range of 1 wt.%, 2 wt.% and 3 wt.% and 1 wt % of PAN was also used as the binder. This mixture was formed into pellets before sintering under the selected pressing force of 17.2369 MPa (2500 psi). These pellets were sintered at 1400°C, 1450°C, and 1500°C sintering temperatures, respectively, with a sintering time of 5 hours for each temperature.

As a result of liquid phase sintering processes, the effect of sintering temperature and the effect of the amount of sintering aid additives were determined by using characterization methods for mullite-zircon system. Some properties of the sintered samples with and without sintering aid addition including porosity, hardness, density, water absorption, shrinkage measurements and microstructural and XRD analysis of the product for sintering temperatures of 1400°C, 1450°C, and 1500°C.

Generally, it was observed that as the temperature increases the porosity decreases, and the densification was improved. No clear reaction products or bonding was identified and a phase formed between iron oxide and the Mullite –Zircon mixture. An increase in the hardness values was observed with the addition of 2 wt.% and 3 wt.% iron-oxide for the temperature of 1450°C and 1500°C. 1 wt.% iron-oxide addition to the sample has a negative effect on the hardness of the material. Sintering aid additive iron-oxide provides the best positive effect on the density for the addition of 1 wt.%- 2 wt.% at 1450°C, but higher addition may have a negative effect on the mullite-zircon mixture.

In conclusion, it was found that an increase in sintering temperature and Fe_2O_3 sintering aid addition into the Mullite-Zircon mixture led to promoting sintering and reducing the porosity. These results suggest that Fe_2O_3 addition has a positive effect on the densification of the microstructure and improvement of the physical and mechanical properties.

SYMBOLS

°C : Celsius degree

rpm : Revolutions per minute

psi : Pounds of force per square inch of area

mm : Milimeter

cm : Centimeter

nm : Nanometer

A° : Angstrom

h : Hour

kcal : Kilocalorie

K_{IC} : Fracture toughness

W : Watt

kg : Kilogram

g : Gram

± : Plus-minus sign

GPa : Gigapascal

Mpa : Megapascal

Ø : Diameter

µm : Micrometer

N : Newton

λ : Wavelength

ρ : Density

P : Force

HV **:** Vickers Hardness

% **:** Percent

> **:** Greater-than sign

≈ **:** Almost equal to

ABBREVIATIONS

ASTM **:** American Society for Testing and Materials

CMCs **:** Ceramic Matrix Composites

deg **:** Degree

MMCs **:** Metal Matrix Composites

Oc **:** Octahedral chains

PMCs **:** Polymer Matrix Composites

PVA **:** Polyvinyl alcohol

PAN **:** Polyacrylonitrile

XRD **:** X-Ray Diffraction

LIST OF FIGURES

Figure 1.1 Composite types 2
Figure 1.2. Mullite crystal structure 3
Figure 1.3. The binary system Al_2O_3-SiO_2. From Aksay and Pask, Science, 183, 69 (1974) 4
Figure 1.4. The structure of zircon 7
Figure 1.5. Phase diagram by Toropov Galakov 8
Figure 3.1 Raw material Mullite-Zircon phase analysis before sintering XRD graph, Mullite (M), Zircon (Z), Cristobalite (C). 14
Figure 3.2 Raw material Iron-oxide Fe_2O_3 phase analysis before sintering XRD graph, Iron-oxide (F). 15
Figure 3.3 Mullite-Zircon + Fe_2O_3 + PAN powder mixtures before the sintering. 16
Figure 3.4 Hydraulic press for compaction process. 16
Figure 3.5 Samples on an alumina plate were placed in the furnace before sintering. 17
Figure 3.6. Nabertherm sintering furnace. 18
Figure 3.7 (a) Samples before sintering, (b) samples after sintering 18
Figure 3.8 (a) Epoxy and Curing liquid, (b) samples in epoxy mold. 19
Figure 3.9 Struers Tegramin 25 grinding and polishing device. 20
Figure 3.10. Diffraction of X-Rays by planes of atoms (A-A' and B-B'). 20
Figure 3.11 Grinding of samples for XRD analysis using mortar and pestle. 21
Figure 3.12 X-Ray diffractometer Bruker AXS, D2 Phaser. 22
Figure 3.13. Samples boiling in distilled water. 23
Figure 3.14 Weighing of samples using Archimedes setup. 23
Figure 3.15 Vickers hardness indent is shown on the sample. 25
Figure 3.16 Vickers indent diagonals. 26
Figure 3.17 Emcotest DuraScan Vickers Hardness device. 27
Figure 3.18 Nikon Epiphot 300 optical microscope. 27
Figure 4.1 XRD graph of Mullite-Zircon without Iron-Oxide addition sintered at 1550°C. Mullite (M), Zircon (Z). 29
Figure 4.2 XRD graph of Mullite-Zircon structure sintered at 1500°C with the addition of Iron-Oxide 0%,1%,2%, and 3% respectively. Mullite (M), Zircon (Z), Cristobalite (C). 30
Figure 4.3 XRD graph of Mullite-Zircon structure sintered at 1450°C with the addition of Iron-Oxide 0%, 1%, 2%, and 3% respectively. Mullite (M), Zircon (Z), Cristobalite (C). 31

Figure 4.4 XRD graph of Mullite-Zircon structure sintered at 1400°C with the addition of Iron-Oxide 0%,1%,2%, and 3% respectively. Mullite (M), Zircon (Z), Cristobalite (C). 32
Figure 4.5 XRD graph of Mullite-Zircon structure sintered at the temperature of 1550°C, 1500°C, 1450°C, and 1400°C respectively. Mullite (M), Zircon (Z), Cristobalite (C).....33
Figure 4.6 Bulk density g/cm^3 – Additive % graph.....34
Figure 4.7 Porosity (%) - Additive (%) graph. 35
Figure 4.8 Vickers Hardness (HV) – Additive % graph.....36
Figure 4.9 Shrinkage (%) - Additive (%) graph. 37
Figure 4.10 Water absorption (%) - Additive (%) graph.....38
Figure 4.11 1550°C sintered mullite-zircon microstructure without iron-oxide addition with magnification 50x.....39
Figure 4.12 1500°C sintered mullite-zircon microstructure with iron-oxide addition (a) 0 wt.%, (b) 1 wt.% (c) 2 wt.% (d) 3 wt.%, with magnification 50x.....40
Figure 4.13 1450°C sintered mullite-zircon microstructure with iron-oxide addition (a) 0 wt.%, (b) 1 wt.% (c) 2 wt.% (d) 3 wt.%, with magnification 50x.....40
Figure 4.14 1400°C sintered mullite-zircon microstructure with iron-oxide addition (a) 0 wt.%, (b) 1 wt.% (c) 2 wt.% (d) 3 wt.%, with magnification 50x.....41

LIST OF TABLES

Table 1.1. Physical properties of mullite ceramics. 6

Table 1.2. Physical properties of normal zircon. 7

Table 3.1. Weight % composition of Mullite-Zircon (MZ) + Fe_2O_3 mixture..... 15

1. INTRODUCTION

1.1. Definition of Ceramics

Ceramic materials are defined as solid compounds that are formed by the application of heat and are dependent on the conditions of heat and pressure. The other element or elements may be either a metal or a non-metallic solid [1]. The alternative definition of ceramics is provided by W. D. Kingery, who defines ceramic materials as "the art and science of making and using solid articles that have inorganic nonmetallic materials as their essential component and are composed in large part of such materials" [2].

Throughout human history, materials have been the predominant factor in determining the competitiveness of individuals and societies. Currently, knowledge of the structure of materials is required for new developments of materials and enhancement. As a result, specific applications to address industrial and societal dares in today's highly competitive world. In this process, ceramic technology is crucial, and as a result, it has emerged as a driver of technological advancement in various industrial sectors [3].

Ceramic materials are hard, brittle, and resistant to wear, susceptible to thermal shock, refractory, thermally and electrically insulate, naturally transparent, nonmagnetic, chemically stable, and oxidation-resistant. There are exceptions; some ceramics are electrically and thermally conductive, and some are even superconductors [1].

The majority of the focus is on the fact that ceramic materials are typically harder, denser, lighter, and more resistant to heat and corrosion than metals. The most fundamental and prevalent issue with ceramic materials is their fragility. This is an extremely difficult problem to solve, but engineers and scientists continue to search for a solution. In the process, scientists have created unheard-of ceramic compounds and applications that meet specific, stringent requirements, such as in the electronics industry [4].

In the scope of the progress made in the 20^{th} century, it is appropriate to divide ceramic into two classes:

1. Traditional ceramics: Traditional ceramics are usually found in monolithic form. These include bricks, pottery, tiles, etc.
2. Advanced ceramics: They usually represent an advanced class of ceramic materials, in which complex chemical processing methods are used to get them. Some examples of mentioned advanced ceramics include oxides, nitrides, and carbides [5].

1.2. Ceramic Matrix Composites

In materials with different physical and chemical properties, the structure consisting of the combination of the other phase dispersed in one phase is called a composite. The main phase is called the matrix, and the phase dispersed in the matrix is called the reinforcement material. When these two phases come together, the resulting material usually shows better properties than the previous ones.

In the matrix, the additive material may exist in various forms, such as particles, whiskers, short fibers, continuous fibers, or sheets. It is often convenient to classify different types of composites according to the matrix material properties, namely polymer matrix composites (PMCs), metal matrix composites (MMCs), and ceramic matrix composites (CMCs) [5].

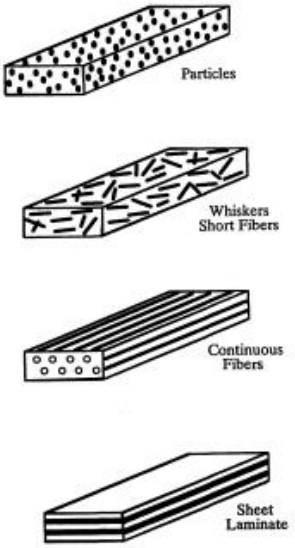


Figure 1.1 Composite types *[5]*.

The reinforced material can be found as metal, ceramic, or polymer in a matrix. Metals containing particles made of ceramic, whiskers, or fibers are gaining prominence as well [5]. Most commercially used composites are polymeric-based matrices; however, both MMCs and CMCs are of great interest in high-temperature applications.

There is a need to develop more robust new materials in various strategic areas to meet the challenges and needs of materials application in the twenty-first century. To meet these needs, the use of ceramic matrix composites offers great advantages [6].

Ceramic matrix composites (CMCs) are materials in which the additive material is dispersed in a ceramic matrix. These composites are brought together considering the high strength, hardness, and thermal stability of the ceramic phase, which is the matrix, as well as the superior characteristics of the additive. Due to their incomparable properties, ceramic

matrix composites are useful for an extensive application range such as cutting tools, dental applications, thermal coatings, nuclear materials, energy, military, aerospace, and building industries [5].

In this study, Mullite-Zircon mixture will be employed therefore each ceramic raw materials will be briefly introduced separately below.

1.3. Mullite

Mullite is silicate made up of chains of AlO_6 octahedra with an orthorhombic structure parallel to the z-axis and cross-linked by tetrahedra containing the elements of Si and Al [7].

Mullite is a material with strength at higher temperatures, creep resistance, low thermal expansion, low dielectric constant, and excellent chemical stability. These characteristics make mullite an excellent material for electronic and structural applications [8].

These characteristics prompted extensive research in the field of refractory and ceramic materials for high-temperature applications. At room temperature, however, monolithic mullite bodies exhibit both low strength and low fracture toughness. In addition, sintering is difficult when there is no glassy phase [9].

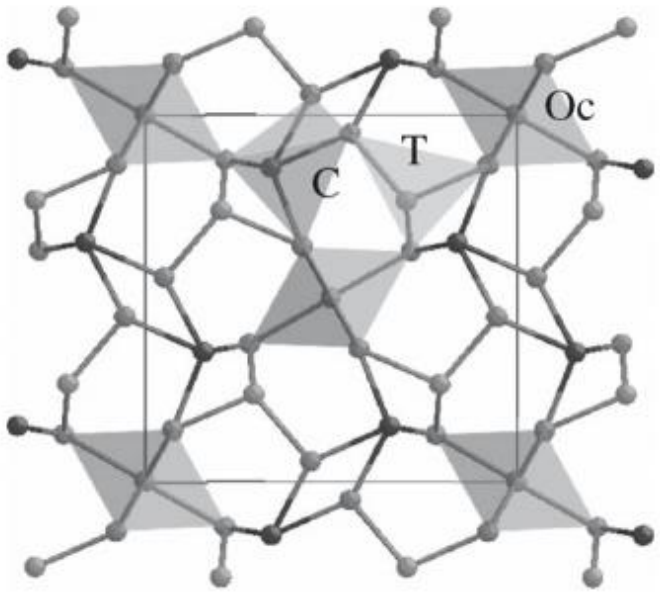


Figure 1.2. Mullite crystal structure *[7]*.

In Figure 1.2. these octahedra chains (Oc) are seen in the corners and center of the unit cell and flow into paper; The two parallel chains are rotated to each other accordingly. Although it seems to be one in this projection, C is not a tetrahedron; T is a tetrahedron [7].

In order to take into account high-temperature phenomena in ceramic systems, an example of the usefulness of phase diagrams, the Al_2O_3-SiO_2 system shows many features and problems encountered.

In this system, mullite is shown as melting incongruently. The eutectic between mullite and cristobalite occurs at 1587°C to form a liquid containing about 95 mole %SiO_2. The temperature of solidus is 1828°C between the mullite compound and alumina compound.

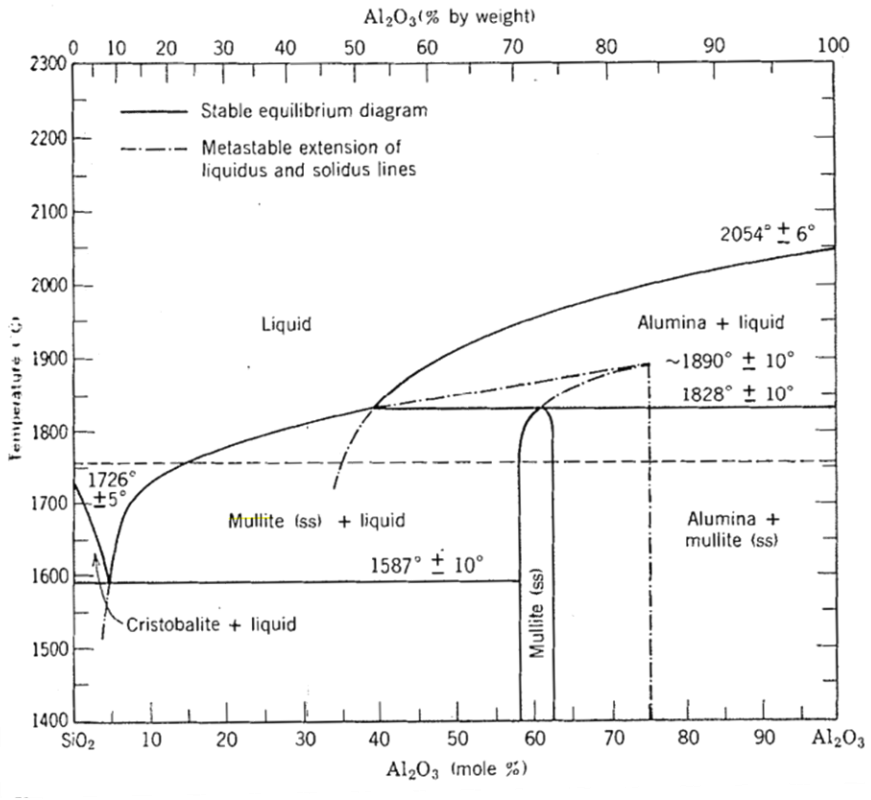


Figure 1.3. The binary system AI_2O_3-SiO_2. From Aksay and Pask, Science, 183, 69 (1974) *[2]*.

This diagram may contain factors that influence the production and application of refractory products. They consist of refractory silica brick (0.2 to 1.0 wt.% Al_2O_3), clay products (35 to 50 wt.% Al_2O_3), high-alumina brick (60 to 90 wt.% Al_2O_3), pure fused mullite (72 wt.% Al_2O_3), and pure fused or sintered alumina (> 90 wt.%).

Brick's refractory properties can be enhanced by adding enough alumina to increase the proportion of mullite until, at more than 72 weight percent alumina, the brick is either entirely mullite or a mixture of mullite and alumina. In this circumstance, no liquid is

produced until the temperature exceeds 1828°C: In certain applications, mullite brick is fused. Mullite brick has exceptional resistance to corrosion and deformation at high temperatures [2].

Mullite's formation, phase purity, and morphology are dependent on its precursor materials and processing history. First identified as the result of heating kaolinitic clays, mullite has an approximate alumina-to-silica molar ratio of 3:1. This is how the reaction proceeds [10].

$Al_2Si_2O_5(OH)_4$	450°C →	$2(Al_2O_3 \cdot 2SiO_2) + 2H_2O$
Kaolinite		Metakaolin
$2(Al_2O_3 \cdot 2SiO_2)$	925°C →	$2Al_2O_3 \cdot 3SiO_2 + SiO_2$
Metakaolin		Silicon spinel
$2Al_2O_3 \cdot 3SiO_2$	1100°C →	$2(Al_2O_3 \cdot SiO_2) + SiO_2$
Silicon spinel		Pseudomullite
$3(Al_2O_3 \cdot SiO_2)$	1400°C →	$3Al_2O_3 \cdot 2SiO_2 + SiO_2$
Pseudomullite		Mullite + Cristobalite

According to the phase diagram, a silica-rich glassy phase in 3:2 mullite is foreseen when it is sintered at higher temperatures than the eutectic temperature of 1587°C. Commonly 3:2 mullites are sintered at a temperature between 1600°C and 1700°C. It may comprise a glassy phase in the microstructure [2].

Materials with a 2:1 mullite alumina content can be completely melted above 1960°C and then cooled to approximately 1890°C without crystallization. Using the Czochralski method, infrared-transparent mullite single crystals could be grown at the aforementioned temperature [10].

According to Pask (as cited in D.J. Duval et al., 2008), mullites with higher molar ratios of alumina to silica (i.e., >3:1) were produced by melting the constituents above the liquidus and quenching. Fusion-produced mullite is typically weaker than sintering-produced mullite.

Mullite powder can be obtained by a variety of means, including crystallization around 1200°C and subsequent sintering at temperatures below the eutectic. Using this method, highly pure mullite and mullite composites were obtained by hot pressing below 1300°C [10].

The exceptional scientific and technical significance of Mullite can be attributed to its high stability of thermal properties and advantageous properties, such as low thermal

expansion and low conductivity, high creep resistance and stability of the corrosion resistance, as well as strength and additionally, fracture toughness (**Table 1.1**) [11].

Table 1.1. Physical properties of mullite ceramics *[11]*.

Properties of Mullite	
Melting point (°C)	≈1830
Density (g cm^{-3})	≈3.2
Linear thermal expansion (×10^{-6} °C^{-1}) 20–1400°C	≈4.5
Thermal conductivity (kcal m^{-1} h^{-1} °C^{-1}) 20 °C	6
Thermal conductivity (kcal m^{-1} h^{-1} °C^{-1}) 1400 °C	3
Strength (MPa)	≈200
Fracture toughness K_{Ic} (MPa m$^{0.5}$)	≈2.5

1.4. Zircon

Zircon is widely used as a refractory material in the steel industry due to its reputation as a good refractory material. Recently, more applications of structural ceramics since highly pure zircon ceramics have numerous desirable properties [12]. Zircon has a wide range of applications and can be used as a material in glass tanks, production of steel, in the industry of energy technology, and as protective coatings for molding tools made of steel. Despite all of the above-mentioned high-temperature applications dependent on a precise understanding of Zircon's thermal stability, the available information on this topic varies greatly in terms of both thermal and chemical properties. Despite the majority of scientific reports agreeing that zircon decomposes via a solid-state reaction, the indicated dissociation temperature varies between 1285 and 1700°C, resulting in different phase diagrams being published [13].

Zircon has a tetragonal structure with a unit-cell structure where a equals to ¼ 6.61 A˚ and c equals to ¼ 5.99 A˚. X-Ray diffraction analysis shows that each zircon atom is surrounded by a tetrahedral group, with 4 oxygen atoms surrounding a central silicon atom (**Figure 1.4.**) [14].

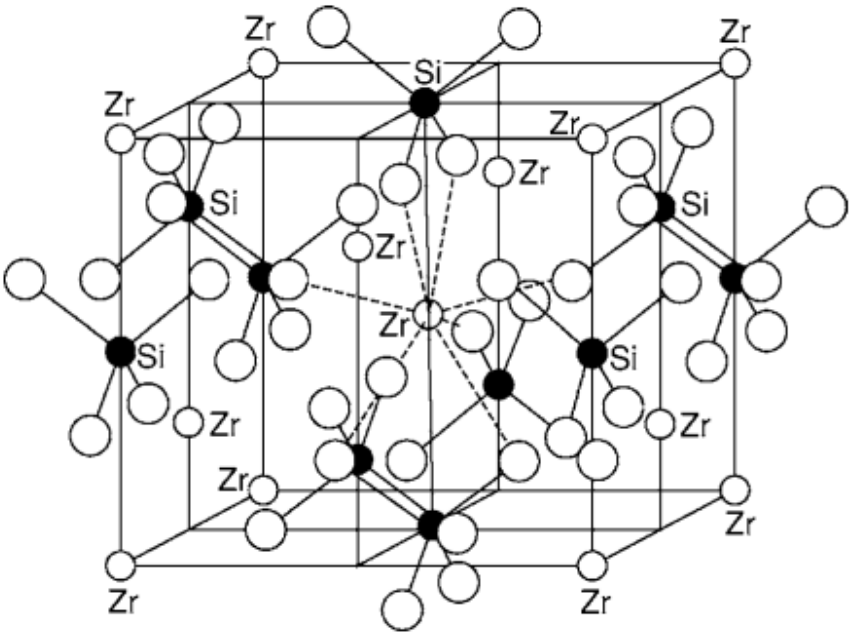


Figure 1.4. The structure of zircon *[14]*.

Zircon contains hafnium material with a ratio of HfO_2/ZrO_2. Zircon is therefore a source of hafnium and also zirconium. Zircons often contain rare earth elements and may be amorphous.

Zircon is a mineral that does contain all of the properties listed, and thus, it is an excellent refractory material. It resists abrasion, impact, thermal shock, and chemical attack, and it has a high melting point (**Table 1.2**) [15].

Table 1.2. Physical properties of normal zircon *[15]*.

Properties of Zircon	
Bulk density (uncompacted) kg/m^3	2643-2804
Specific gravity	4.60-4.71
Mohs hardness	7.0-7.5
Melting point °C	2100-2300
Coefficient of linear expansion cm/cm °C	$7.2x10^{-6}$

Scientists have studied the SiO_2-ZrO_2 system for many years and some following results have been revealed.

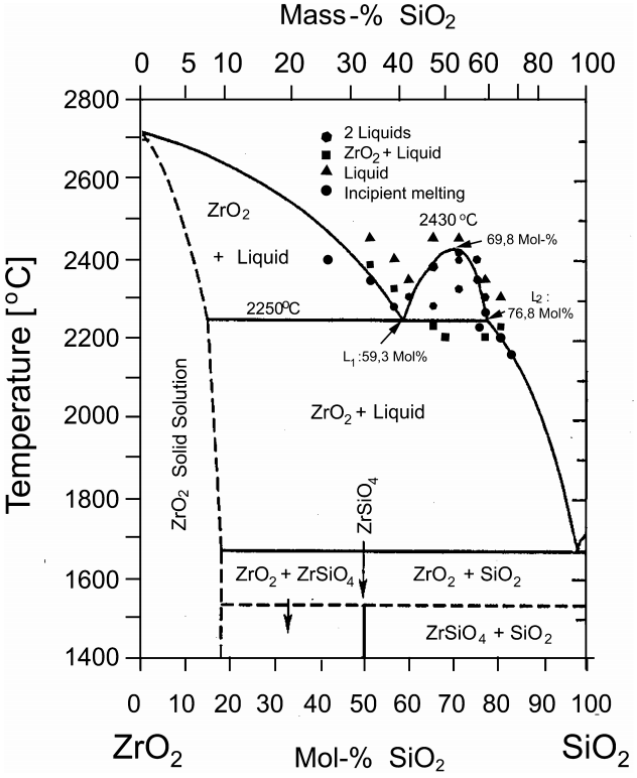


Figure 1.5. Phase diagram by Toropov Galakov *[16]*.

In 1920, Washburn & Libman reported that the melting point of ZrO_2 is in the range of 2700°C, which is still valid today, and that interphase zirconia $ZrSiO_4$ melts at 2550°C [16].

In Barlett's research (1931), pellets were heat treated to 1450°C to determine the stability temperature of zircon, and a liquid phase partition was observed yielding zirconia-rich and silica-rich glasses. Zirconium-rich glass contains monoclinic ZrO_2 and annealing below 1450°C results in zircon formation [16].

In 1934, Zhirnova published a SiO_2-rich eutectic at the temperature of 1705°C and a ZrO_2-rich at a temperature of 2220°C while zircon was considered to melt congruently at 2430°C.

Geller & Yavorski and Geller & Lang established the eutectic reaction between zircon and cristobalite at 1675 ± 5°C in 1945-1949. phase diagram They formed the first phase diagram with the peritectic decomposition of zircon into solid ZrO_2 and liquid SiO_2 at 1775 ± 10°C [16].

In 1956, Toropov & Galakhov researched the liquidus surface of the binary system. By rapidly cooling the sample in the tungsten coil from 2500°C, they found ZrO_2 dendritic crystals with a refractive index of 2.05. They have completed the phase diagram by adding their further conclusions as an extension toward higher temperatures (**Figure 1.5**) [16].

1.5. Mullite-Zircon Composites

Studies have been carried out with ceramic-ceramic composites to improve the performance of ceramic materials. It is known to contribute positively to the properties of ceramic materials.

Zircon undergoes no structural change until its dissociation at approximately 1700 degrees Celsius. With a low thermal expansion coefficient (4.1 x 10-6/°C from room temperature to 1400°C) and a low heat conductivity coefficient (5.1 W/m°C at room temperature and 3.5 W/m°C at 1000°C), it exhibits superior chemical stability and thermal shock resistance. High-purity sintered zircon can maintain its bending strength at temperatures between 1200 and 1400 degrees Celsius. These remarkable properties make zircon a possible candidate for use as a structural ceramic, especially in fields where sudden temperature changes are possible [12].

Mullite's chemical composition varies between $3Al_2O_3–2SiO_2$ and roughly $2Al_2O_3–2SiO_2$. In recent decades, it has received considerable attention as a potential structural material for high-temperature applications [17]. Mullite is an advanced structural and functional material with low thermal expansion, low thermal conductivity, good chemical stability, good creep resistance, and high-temperature resistance [18].

There are several studies on composite materials with zircon as the primary phase, as well as a significant number of studies on composites with mullite. Although zircon and mullite differ chemically and crystallographically, their mechanical properties are comparable [17]. The incorporation of zircon ($ZrSiO_4$) into the matrix of reaction-sintered mullite improves the mechanical and corrosion properties of mullite refractories [18].

1.6. Liquid-Phase Sintering of Ceramics

Liquid phase sintering is a sintering method used to take the final shape of ceramics and metallic powders. The main advantage of this production method is to obtain the product at a low sintering temperature, to ensure rapid densification, and increase its density. It is normal for different microstructures to emerge as a result. This sintering method generally gives better mechanical and physical properties than the solid-state sintering method.

Due to rapid material transport through the liquid, the transformation of microstructure during liquid phase sintering occurs rapidly. Typically, significant condensation occurs in the solid state during heating to the liquid phase sintering temperature; The solid-state sintering step affects the initial microstructure of liquid-phase sintered materials.

During the heating of a compact powder mixture, a liquid phase is formed, and there are fine and canal channels between the solid particles. Due to the pressure difference between the fine and coarse capillaries, the liquid flows into the fine capillaries. This fluid flow can redistribute solid particles, a phenomenon known as "particle rearrangement." As liquid flows into the fine capillaries between the solid particles, the majority of the molten regions of the particles become pores. Elimination of closed pores regulates the overall densification kinetics [19].

This procedure requires the presence of at least two chemical elements. Typically, a mixture of powders with different chemical compositions is employed, with one main component (which is kept solid) and one or more minor components (these minor ones are additives that initiate liquid formation which is known as sintering aids). The liquid can be formed either by melting the additive (in which case the melting point/range must be below the sintering temperature) or by forming a eutectic with a low melting point between the solid phase and the additive at their points of contact [20].

1.7. The Aims of the Project

The mullite-zircon system is a refractory system with high (1500-1550 °C) sintering temperatures. In this study, it is aimed to reduce the sintering temperature by adding a sintering aid additive and using the liquid phase sintering method. As a result of this addition, its effect on the physical and chemical properties and microstructural development of the sintered material will be studied. For this purpose, iron oxide addition with known as flux or sintering aid effect was chosen. As will be explained in the experimental section, it is aimed to find the optimised material properties and lowest cost product to be obtained with the optimum sintering temperature for the parameters used and the amount by addition of the sintering aid additive to be used.

2. LITERATURE SURVEY

The articles reported in the literature regarding the Mullite/Zircon system or iron oxide added ceramic composite materials used in this study are summarized below.

2.1. The Synthesis of Mullite/Zirconia Composite Materials Doped With Boron Minerals.

H. Aydın, in her doctoral dissertation on the synthesis of mullite/zirconia composite materials doped with boron minerals, made a study to synthesize mullite zirconia at low temperatures and to achieve more dense material and better mechanical properties. In this study, colemanite, ulexite, tincal, boric acid, and borax pentahydrate were used as sintering additives. All mixtures were ball milled for 6 hours at 300 rpm speed. Samples were prepared as pellets and bars were then moistened with 3% PVA dissolved water.

For the XRD analysis, all samples were sintered at 1000, 1100, and 1200°C in 3 groups to check the correlation between phase formation and the sintering temperature. Additive-free, colemanite added mixture, and ulexite added mixture were reaction sintered at 1450, 1500, and 1550°C. It was observed that the addition of colemanite and ulexite disintegrated the zircon in samples sintered at 1100, 1000, and 1200 degrees in XRD. The high-density mullite/zirconia composite was sintered at lower temperatures with the addition of boron-based sintering additives. The high-density mullite/zirconia composite was sintered at lower temperatures with the addition of boron sintering additives. This study shows us that the addition of the sintering additives provides better properties on mullite/zirconia composites. After the sintering at 1000, 1100, and 1200°C, disintegrated zircon was not observed in XRD patterns of samples doped with tincal, boric acid, and borax pentahydrate. This is an important inspiration for our study as it shows that the zircon structure can be preserved in other boron additions. The zircon phase can be observed in the structure of the additive-free sample sintered at 1100, 1200, and 1300°C. The mullite formation was observed in the additive-free sample at 1200°C. The zirconia formation starts at 1450-1500° [21].

2.2. Effect of Yttria on Mechanical and Microstructural Properties of Reaction Sintered Mullite-Zirconia Composites

In another research, Das et Al. (1998) studied the effect of Yttria on the mechanical and microstructural properties of reaction-sintered mullite-zirconia composites. The Indian Zircon flour and calcined alumina were ground together for 6 hours with zirconia balls in isopropyl alcohol. Mullite-zirconia composites containing 0, 3, 5, and 7% of Yttria. The slurry from the attritor was dried, granulated by sieving, and uniaxially pressed into bars and discs after the addition of a 10% PVA binder.

The pressed samples were sintered at 1400-1650°C with a 2-hour soaking period. The bulk density and true density were measured. The decomposition of zircon and formation of mullite was observed in Mullite-Zirconia composites containing %3 of Yttria at 1550°C. However, the control composites (additive-free composites) completed the same stages at 1600°C. The control composites reached max relative density at 1550°C whereas Yttria-containing composites reached the highest density at 1500°C. The presence of higher Yttria addition caused heterogeneous microstructure at 1600°C, and 7% containing composites showed low density and porous structure, but Yttria-aided composites showed a lower thermal expansion coefficient. The addition of Yttria helps to decrease the martensitic start temperature.

Yttria-containing samples show the highest fracture toughness of 5.2 MPa $m^{1/2}$ at 1550°C, and maximum hardness (10.1 GPa) was achieved in the composites with 5% yttria addition. The hardness and fracture toughness of the control sample is 5.6 GPa and 3.7 MPa $m^{1/2}$, respectively. As the results show, the addition of Yttria significantly increased the fracture toughness of mullite-zirconia composites, improves mechanical and thermal properties, and decrease martensitic transformation temperature [22].

2.3. Effects of Fe_2O_3 Concentration on Microstructures and Properties of SiC-based Ceramic Foams

In this study, SiC-based ceramic foams' compressive strength and thermal shock resistance properties were investigated by Fe_2O_3 concentration. It was found that as the Fe_2O_3 concentration increased, the number of cyclic thermal shocks of ceramic foams decreased significantly. At room temperature, its compressive strength increased quickly.

Fe_2O_3 concentration plays an important role in the sintering behavior of SiC-based ceramic foams. Raw SiC powders used to prepare SiC-based ceramic foams ineluctably contain Fe_2O_3.

It was observed that the excessive amount of Fe_2O_3 addition can reduce thermal shock resistance properties. In the same sintering process, as Fe_2O_3 concentration increases, the glass phase ratio increases, increasing compressive strength. Fe_2O_3 material can be added to the SiC-based ceramic foams as a sintering aid additive.

High Fe_2O_3 concentration can increase the compressive strength of the SiC ceramic foam at room temperature. But there is a side effect of Fe_2O_3 sintering aid addition which is reducing thermal shock resistance and strength at high temperatures. Therefore, the Fe_2O_3 concentration should be properly controlled [23].

2.4. Low-Temperature Co-Sintering for Fabrication of Zirconia/Ceria Bi-Layer Electrolyte via Tape Casting Using a Fe_2O_3 Sintering Aid

These studies were carried out because the GDC/YSZ bilayer electrolyte is known to be problematic due to its thermochemical instability at high sintering temperatures. First, they match the tensile profile of the two bulk materials by using Fe_2O_3 sintering aid additive. During co-sintering, adding 5% moles of Fe_2O_3 to the GDC and 2% moles of Fe_2O_3 to the YSZ prevent delamination. The addition of Fe_2O_3 inclines densification by providing a dense double layer at a reduced sintering temperature of 1300°C, the temperature 150°C below the essential sintering temperatures.

When Fe_2O_3 was used elemental analysis shows the composition distribution curves along the bilayer interface were asymmetrical. Fe_2O_3 increases the overall conductivity of the bilayer electrolyte by an order of magnitude. Bi-layered 8YSZ/GDC10 was produced by using the tape casting method at a reduced sintering temperature of 1300 ◦C. Microstructural defects and delamination were not encountered. The total conductivity of two-layer electrolytes containing Fe_2O_3 is 1.5 times that of a single-layer 8YSZ electrolyte. This study shows that cost-effective wet ceramic manufacturing methods such as tape casting can be used for bilayer electrolyte cell fabrication [24].

3. EXPERIMENTAL STUDIES

3.1. Raw Materials

3.1.1. Mullite-Zircon

In this study, a Mullite-Zircon mixture ($3Al_2O_3 \cdot 2SiO_2$+ $ZrSiO_4$) supplied from a Local refractory factory in Istanbul was used to form the matrix. The mixture contains 60% Mullite ($3Al_2O_3 \cdot 2SiO_2$) and 40% Zircon ($ZrSiO_4$) by weight. The grain size of the mixture was controlled to be below 63µm. Mullite-zircon mixture before sintering X-ray Diffraction graph was depicted in **Figure *3.1***.

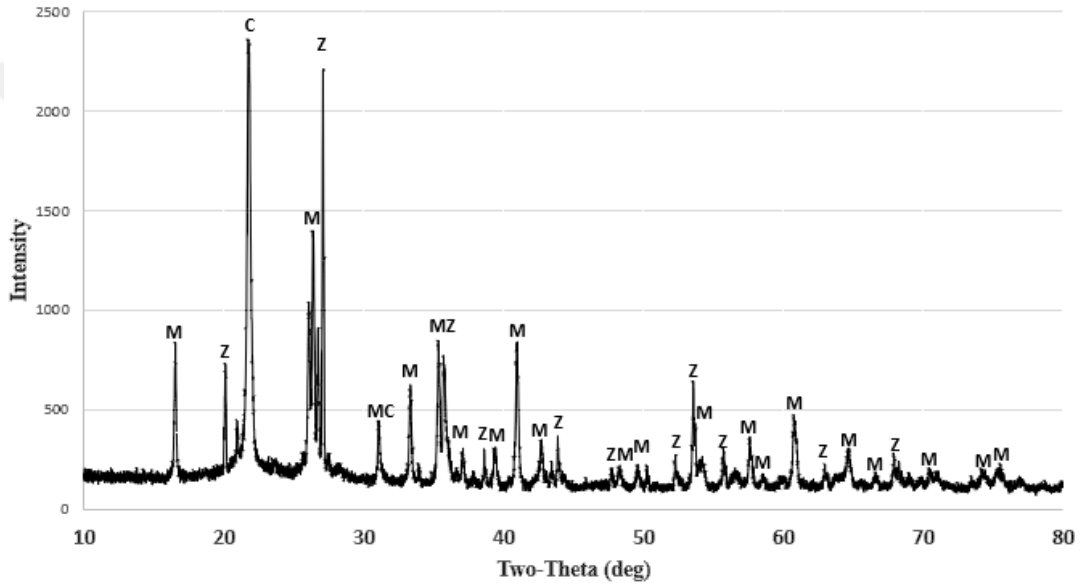


Figure 3.1 Raw material Mullite-Zircon phase analysis before sintering XRD graph, Mullite (M), Zircon (Z), Cristobalite (C).

3.1.2. Binder

PAN (Polyacrylonitrile) was used (1 wt.%) as a binder to reduce the friction forces during compaction of the pellets.

3.1.3. Iron Oxide

Iron oxide or hematite (Fe2O3) used as a sintering aid additive which was supplied from a Local refractory plant in Istanbul. The grain size of the iron oxide powder was controlled to be below 63µm. The X-ray Diffraction peaks of iron oxide was shown in **Figure *3.2***

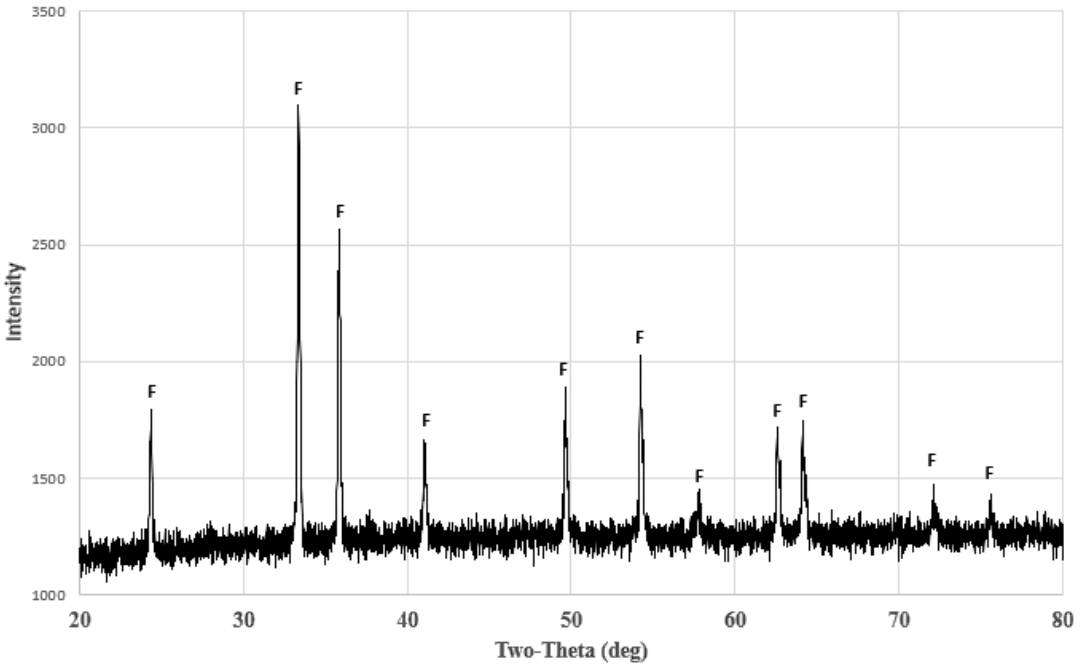


Figure 3.2 Raw material Iron-oxide Fe_2O_3 phase analysis before sintering XRD graph, Iron-oxide (F).

3.2. Preparation of Powders

In this study, two different products were prepared with and without sintering aid additives. The test or reference sample contains only mullite-zircon whereas Fe2O3 was added into the mullite-zircon batch at range of 1wt%, 2wt%, and 3wt% by mass for sintering aid added products. In addition, 1% by weight of PAN (Polyacrylonitrile) was used as a binder. For each mixture, the materials were weighed in such a way that 1 wt.% PAN was added to the total weight. The contents of the prepared products are given in the table below (**Table 3.1**)

Table 3.1. Weight % composition of Mullite-Zircon (MZ) + Fe_2O_3 mixture.

MZ (wt.%)	Fe_2O_3 (wt.%)
100	0
99	1
98	2
97	3

The mixing process was applied in a ball mill for 90 minutes for mechanically mixing of these each prepared mixtures. These mixtures are the batches ready for the next compaction step to produce pellets which is shown in **Figure *3.3***.

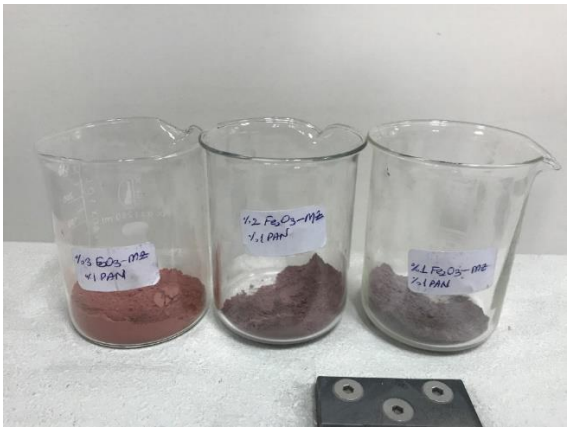


Figure 3.3 Mullite-Zircon + Fe_2O_3 + PAN powder mixtures before the sintering.

3.3. Compaction of the Powder Mixture

After the ball milling mixing process, the mixture needs to be shaped to carry out the microstructural evaluation and as well as physical, mechanical tests and bring it into a suitable shape for sintering. The mixtures were weighed before shaping using a precision balance so that each pellet was 2 grams. In the compaction process, a hydraulic press with a 25 mm diameter cylindrical hardened steel mould were used (**Figure *3.4***)



Figure 3.4 Hydraulic press for compaction process.

These powders with and without a sintering aid, weighing 2 grams, were put into the mold and kept under a load of 17.2369 MPa (2500 psi) for 20 seconds and formed into cylindrical pellets. 2-gram pellets with a diameter of 25 mm were obtained and prepared for the sintering of the product.

3.4. Sintering

The sintering process was carried out on an alumina plate and covered by pouring alumina powders on the plate, preventing the risk of sticking in the samples (**Figure 3.5**). It is intended to sinter only the test sample containing mullite-zircon at 1550°C. Apart from that, the temperatures tested for samples containing sintering aid additive (Fe_2O_3) are 1400°C, 1450°C, and 1500°C, respectively. Test specimens containing mullite-zircon and binder (PAN) were sintered at every specified or desingnated temperature (1400°C, 1450°C 1500°C and 1550°C). Sintering was performed using Nabertherm (Germany) furnace heated by electrical resistance in air (**Figure 3.6**).



Figure 3.5 Samples on an alumina plate were placed in the furnace before sintering.

Binder (PAN) that aids in shaping should not be present in the structure of the sample after sintering. Therefore, binder removal should be performed to remove the binder (PAN) in the mixture slowly from the sample. In order to remove the binder from the structure, the furnace at room temperature (25°C) was heated to 600°C at 2°C/min. When the pellets reached at 600°C in about 5 hours, then they were kept at this temperature for 2 hours for binder removal..

After the binder removal from the sample, then sintering process was started with a heating rate of 10°C /minute up to the designated sintering temperature. When it reached the pre-determined sintering temperature, it remained at this temperature for 5 hours and the sintering process was completed. Finally the furnace was left to cool itself naturally for 24 hours to room temperature.



Figure 3.6. Nabertherm sintering furnace.

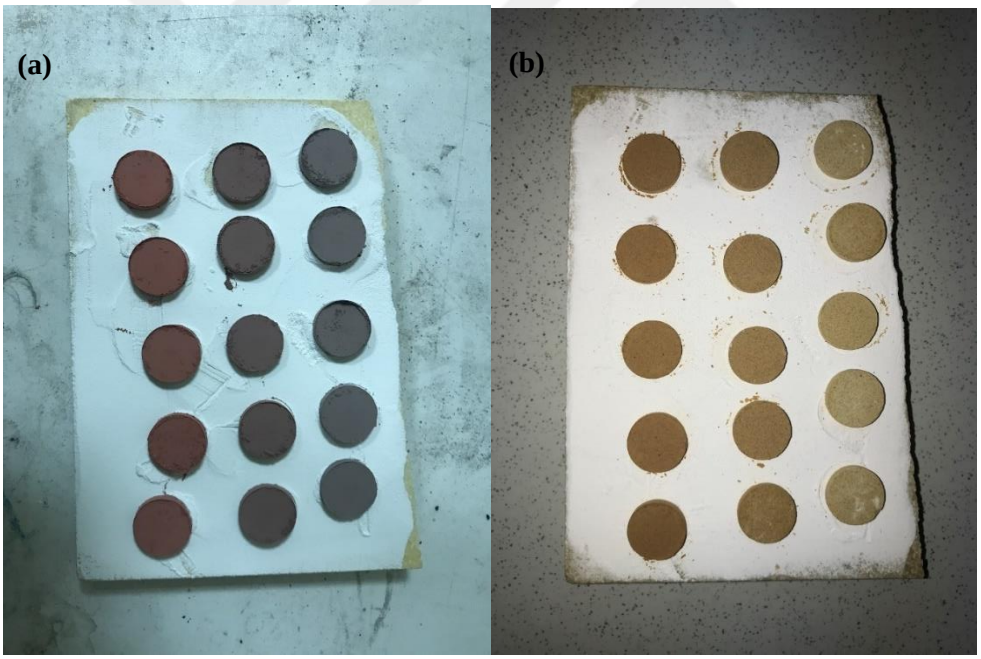


Figure 3.7 (a) Samples before sintering, (b) samples after sintering

3.5. Characterization of Samples

3.5.1. Sample preparation for ceramography and hardness test

Mechanical preparation is a commonly used technique to prepare samples for microscopic analysis. In order to remove material from the surface until the desired result is achieved, the samples are prepared so that the abrasive particles are finer with each step and for a certain period. The purpose of molding the sample is to prepare the samples for analysis such as hardness testing and microstructural evaluation.

The sintered samples prepared in this study were taken into an epoxy mold with a diameter of 40 mm. Akasel brand Aka-Resin Liquid Epoxy (No: 25101115 (8510)) and Aka-Cure Slow (No: 25101211 (8550) were used for molding. After the epoxy was cured, the samples became ready for the grinding and polishing stages (**Figure *3.8***).

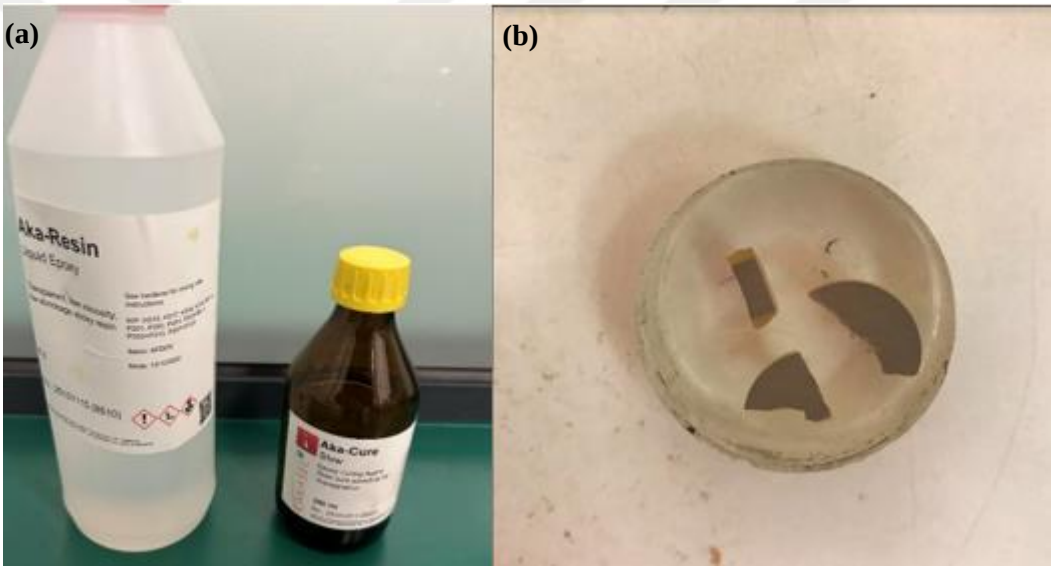


Figure 3.8 (a) Epoxy and Curing liquid, (b) samples in epoxy mold.

The polishing process was carried out in 3 stages. Struers brand Tegramin 25 model polishing device was used in the polishing process (**Figure *3.9***). Coarse grinding was conducted using Struers Piano 220 machine under 30N force using a 300 rpm table and 150 rpm holder parameters with water for 3 minutes and prepared for the next step. In the next stage, 150N force was applied to the holder and table under 30 N force using Struers brand Allegro and using 9µm grain size diamond suspension with Akasel brand DiaMaxx Poly. Samples were polished for 4:30 minutes in these parameters. In the final polishing stage, 150N force was applied to the sample holder and table under 30 N force, Akasel brand DiaMaxx Poly 3µm grain size diamond suspension, and the Struers MD-Dac were used as polishing instruments. Samples were processed for 3 minutes under this condition.



Figure 3.9 Struers Tegramin 25 grinding and polishing device.

3.5.2. XRD analysis of powders

X-rays are electromagnetic radiation with short wavelengths and high energies proportional to the atomic ranges of solids. When the x-ray beam strikes a material, a portion of the beam is scattered in all directions by the electrons interacting with each ion and atom in the beam's path shown in **Figure *3.10*** [25].

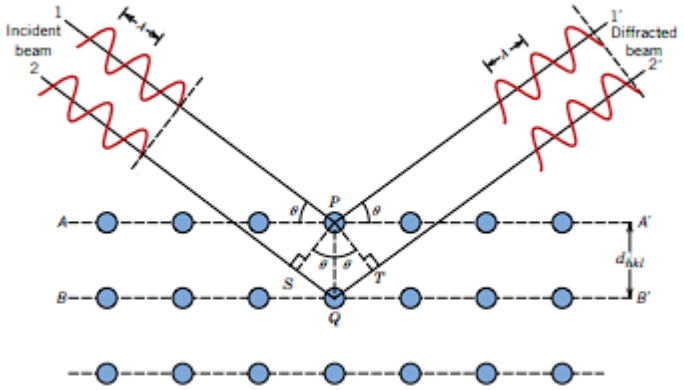


Figure 3.10. Diffraction of X-Rays by planes of atoms (A-A' and B-B') *[26]*.

This equation is known as Bragg's law; in this formula, n is the reflection, which can be the integer (1, 2, 3, . . .) viable with sin θ not surpassing unity.

$$n\lambda = d_{hkl} \sin\theta + d_{hkl} \sin\theta = 2d_{hkl} \sin\theta \qquad (\mathbf{3.1})$$

This method of non-destructive analysis is used to determine the crystallographic properties of the materials and the phases present in the structure. By applying X-ray diffraction to powder samples, it is possible to determine grain size and orientation in addition to the crystal structure.

In order to obtain and analyze the peaks of X-Ray diffraction, samples were ground in mortar when the particles sufficiently fine (-63 μm) for the analysis (**Figure 3.11**). In this study, raw mullite-zircon, raw Fe_2O_3, and sintered samples both with and without sintering aid addition were analysed using an XRD device.



Figure 3.11 Grinding of samples for XRD analysis using mortar and pestle.

In this study, X-Ray diffraction analysis was performed using Bruker AXS, D2 Phaser (Germany) (**Figure 3.12**). The parameters are as follows,

Lambda (λ): 1.54184 Å
Scanning range: 10°-80°



Figure 3.12 X-Ray diffractometer Bruker AXS, D2 Phaser.

3.5.3. Density and porosity and shrinkage measurements

In most ceramic systems, especially in high-strength or high-temperature applications, the density and porosity of the materials is critical. The main reason for this is that porosity affects the strength, elasticity, thermal properties, and corrosion and mechanical wear behavior of a material. The method used for density measurement is based on the Archimedes principle and is a widely used system for measuring the density of solid materials.

The volume of pores in a sample is calculated based on the amount of liquid required to fill them. Although the majority of open pores can be filled by the liquid used in this analysis, some pores can be closed; these closed pores are not included in the calculated value because the liquid cannot fill them. The calculated porosity and solid density values are therefore referred to as apparent porosity and apparent solid density.

According to ASTM C373-18, to perform this measurement, balance (weight accurately to 0.01g), a furnace capable of maintaining a temperature of 150°C ± 5°C, a wire, basket, or halter for making suspended mass measurements, a glass beaker such size and shape that the sample, wire loop can suspend in the water and the beaker or container will not contact with any sample or wire loop. In addition to this system, there is a need for the pan to boil samples and distilled water should be used as a liquid [27].

The dry weights of the samples were weighed on a precision balance and recorded for the calculation step. After this stage, distilled water and sintered materials were put into the beaker. The samples were left in boiling distilled water for 1 hour (**Figure 3.13**). After the samples were cooled down to room temperature in distilled water, samples were taken one by one from the distilled water to the prepared mechanism in order to perform Archimedes' principle.



Figure 3.13. Samples boiling in distilled water.

First, the suspended weights of the boiled and cooled samples in water were weighed (**Figure 3.14**). Then, after it was removed from the apparatus, the excessive water on the surface was removed with the help of paper. Then, the water-absorbed weights of sintered samples were weighed immediately.



Figure 3.14 Weighing of samples using Archimedes setup.

The results were recorded for the next step, calculations. This process was carried out on 3 samples for each composition and temperature. The results were obtained by putting the obtained data into the given formula. Results are given as the average of 3 test samples. The formulas used and their definitions are as follows.

(1) $V = M - S$ **(3.2)**

(2) $B = D / V$ **(3.3)**

Where,

V: exterior volume in cubic centimeters

M: saturated mass, g

S: mass of the sample suspended in the water, g

B: bulk density, g/cm^3

D: mass of the sample in dry condition, g

This method is allowed us to measure density and porosity results and make a comment on how the sintering aid affected mullite-zircon structure at different sintering temperatures.

For the measurement of shrinkage in the surface area, volume and the diameters of the specimens known before sintering were measured after the sintering process. The diameters of the samples before sintering are equal to the diameter of the mold and are 25 mm. Calculations to find the surface area shrinkage were made with the formula given below.

$$D_S = \left(\frac{D_i - D_f}{D_i}\right) \times 100 \quad \textbf{(3.4)}$$

Where,

D_S: surface area shrinkage, %

D_i: initial diameter, mm

D_f: diameter after sintering, mm

3.5.4. Hardness test

Hardness can be expressed as resistance to friction, scratching, shearing, or plastic deformation under static or dynamic loading conditions.

In other words, hardness is a measure of the material's resistance to plastic deformation. Hardness tests were previously carried out according to the ability of two materials to scratch each other, and a scale was formed as a result of these. In this scale, the relative hardness of the materials could be seen. This scale is called the Mohs scale. In this method, the hardness values on the scale range from 1 to 10. 1 is the hardness value of talc and 10 is the hardness value of a diamond. Other materials take values between 1-10 [25].

Vickers hardness method have been developed for more countable values. This hardness measurement method gives information about the hardness of the material in ratio to the depth or width of the indent formed by immersing a tip into the material [25].

The Vickers Hardness Test employs a diamond pyramid with a square base. It is also referred to as the diamond pyramid by Vickers. Methodically, Vickers and Knoop are comparable. In both methods, the diamond measuring tip is dipped into the surface of the sample to determine its hardness. It involves immersing a diamond, square pyramid-shaped tip with an angle of 136 degrees on the surface of the piece of material whose hardness is to be measured, under a certain load, for a certain period, and measuring the diagonals to determine the trace area formed after the load is removed. The Vickers hardness value is the ratio of load to indentation surface area.

Vickers hardness number, HV, n- an expression of hardness derived by dividing the force applied to a Vickers indenter by the surface area of the permanent impression produced by the indenter.

In contrast to conventional bulk indentation hardness tests, this test method determines a material's hardness based on the formation of a very small indentation using a relatively low force.



Figure 3.15 Vickers hardness indent is shown on the sample.

Using a specially designed testing machine, a Vickers indenter made from a diamond with a specific geometry is pressed into the test specimen surface with a force in the range of 1 to 1000 g. Using a light microscope with a filar-type eyepiece or another measuring instrument as shown in**Figure *3.15***, the size of the indentation is determined.

The Vickers hardness number is de from the force divided by the indentation's surface area. It is assumed that elastic recovery does not occur when the indenter is removed after the loading cycle, or that the indentation retains its original shape after the force is removed.

In the Vickers hardness test, a pyramid indenter with a square base (**Fig. 3.16**) and opposite sides that meet at the apex at an angle of 136° is used. The indentation shape and formula for calculating Vickers hardness are shown below.

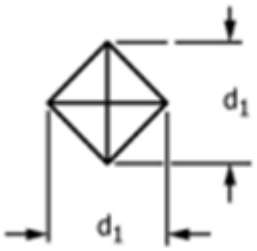


Figure 3.16 Vickers indent diagonals.

$$HV=1.854P/d_1^2 \quad \textbf{(3.5)}$$

In this study, the HV0.2 as load and the 16-second load application time were determined as the parameters for the hardness measurement of the material. Hardness tests were carried out using the Emcotest brand, Duroscan Model 70 device type, and model (**Figure 3.17**). The samples were moulded in an epoxy resin before, and their surfaces were ground and polished for the hardness test. Hardness measurements were performed by taking at least 3 indents from each sample and calculated the average of these results.



Figure 3.17 Emcotest DuraScan Vickers Hardness device.

3.5.5. Microstructural analysis

Microstructural analysis plays an important role in determining physical, chemical and mechanical properties. At the same time, it sheds light on issues such as quality control in production, development of new materials, determination of material properties, and investigation of damage or accident causes caused by materials. In microstructural analysis with a microscope, phases in the material, the number of phases, pores, grain size and shape, and structural defects can be determined.

Microstructure images were taken using Nikon brand Epiphot 300 optical microscope (**Figure 3.18**). Microstructure images were taken from each of the samples at 50x magnification.



Figure 3.18 Nikon Epiphot 300 optical microscope.

4. RESULTS AND DISCUSSIO 27

4.1. XRD Results

The peaks of Mullite and Zircon are visible in the XRD results of the mullite-zircon without Iron-Oxide addition sample sintered at 1550°C.

The pattern of the mullite-zircon structure without the sintering aid of iron-oxide at the sintering temperature of 1550°C only shows mullite and zircon phases. In this study, on X-Ray diffraction graphs, (M) indicates the Mullite phase, (Z) indicates the Zircon phase and (C) indicates the cristobalite phase.

The absence of peaks belonging to the cristobalite phase is apparent when compared to the mullite-zircon samples without sintering aid addition examined at temperatures of 1400°C, 1450°C, and 1500°C.

When XRD results of the mullite-zircon structure without iron-oxide addition were investigated for the samples before sintering (**Figure 3.1**) and after sintering (**Figure 4.1**), the only major change was observed in the cristobalite phase, resulted in the elimination of phase at a higher temperature, 1550°C.

This is a result of the conversion of the cristobalite phase to the glassy phase at 1550°C (**Figure 4.1**).

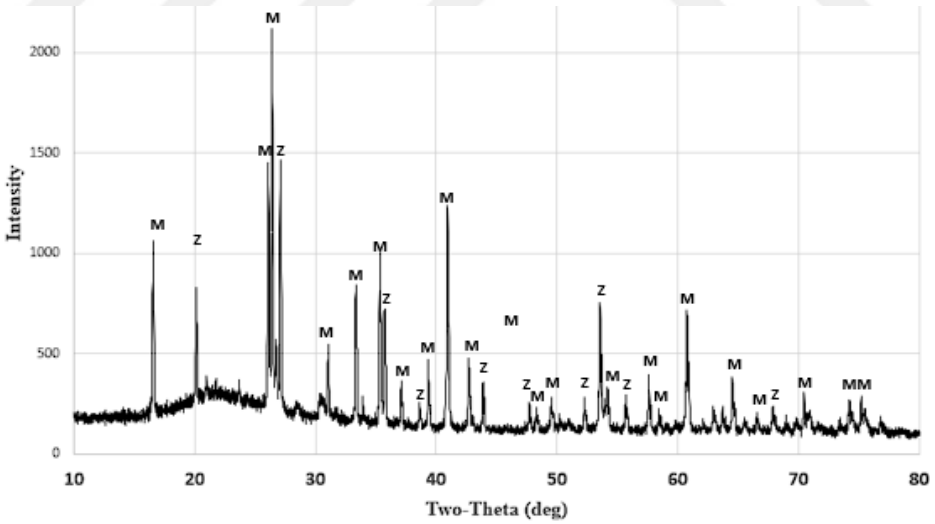


Figure 4.1 XRD graph of Mullite-Zircon without Iron-Oxide addition sintered at 1550°C. Mullite (M), Zircon (Z).

When the mullite-zircon samples with and without iron-oxide sintering aid additive sintered at 1500°C were studied, the iron-oxide peaks could not be visible in the graph changing with the additive, due to the low wt. % of the additive and the overlap of the iron

oxide peaks with the peaks in the mullite-zircon system.

It has been observed that there are peaks of cristobalite in the samples sintered at 1500°C. Cristobalite (SiO_2) is found here at about Two-theta 22° and 31° (**Figure 4.2**).

New phase formation was not observed from the X-Ray diffraction peaks at the sintering temperature of 1500°C with iron-oxide sintering aid addition in a range of 1-3 %.

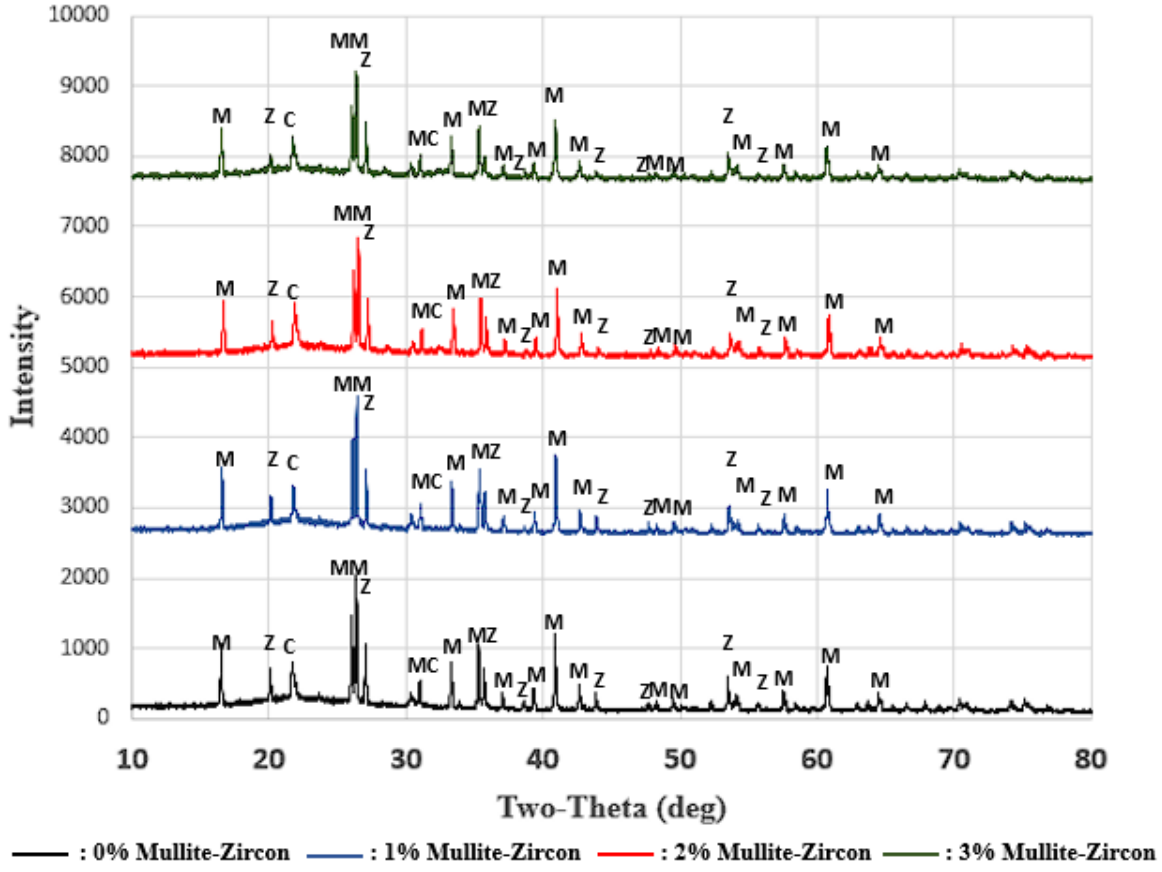


Figure 4.2 XRD graph of Mullite-Zircon structure sintered at 1500°C with the addition of Iron-Oxide 0%,1%,2%, and 3% respectively. Mullite (M), Zircon (Z), Cristobalite (C).

The samples sintered at 1450°C, peaks of the cristobalite phase appear to exist at approximately 22° and 31° on the graph, with the highest intensity value compared to the

samples sintered at 1500°C.

As in other sintering temperatures, the iron-oxide peaks could not be shown in the XRD graph that changes with the wt.% additive, due to low wt.% of the sintering aid addition to the structure and the iron oxide peaks overlap with the peaks in the mullite-zircon system.

With the increase in the weight % of the sintering aid addition (iron-oxide), the peaks of mullite-zircon were observed to be less intense than the sample without the iron-oxide additive (**Figure 4.3**).

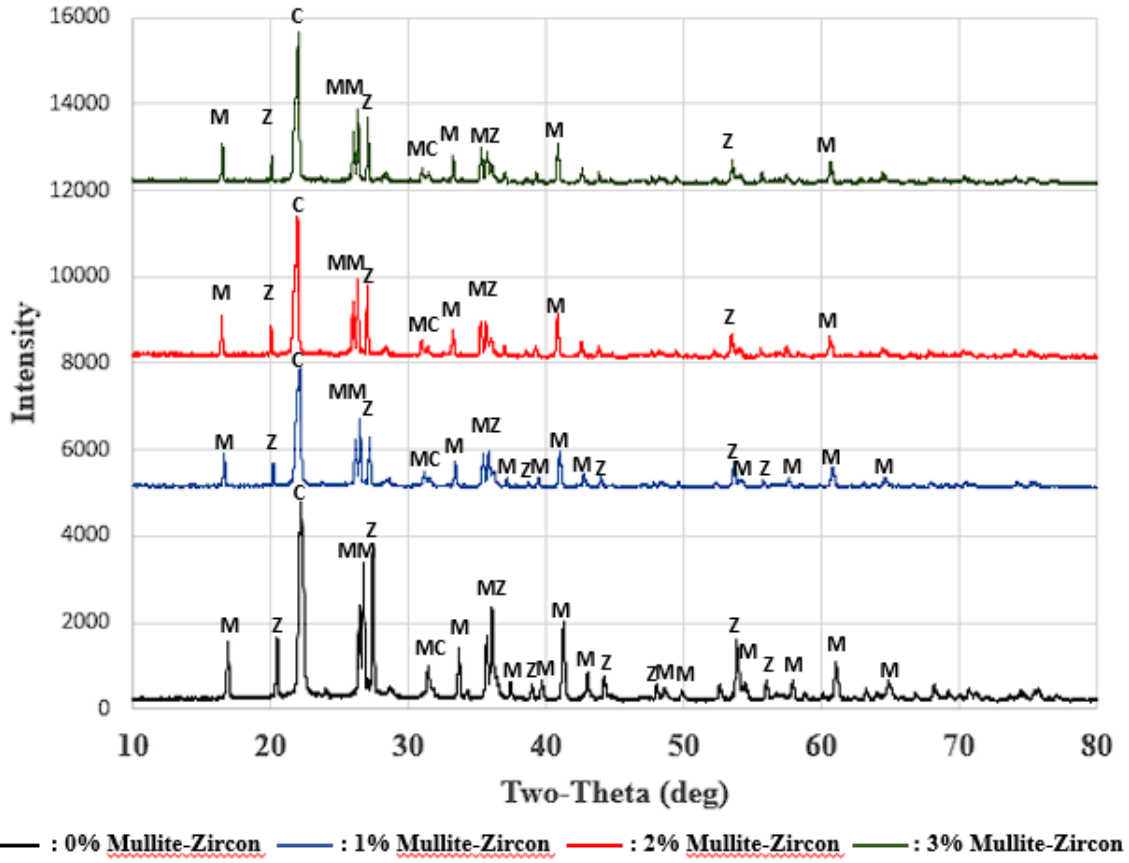


Figure 4.3 XRD graph of Mullite-Zircon structure sintered at 1450°C with the addition of Iron-Oxide 0%, 1%, 2%, and 3% respectively. Mullite (M), Zircon (Z), Cristobalite (C).

The X-Ray Diffraction graph of the samples sintered at 1400°C without additives and with the addition of 1 wt.%, 2 wt.%, and 3 wt.% iron-oxide is as follows. (**Figure 4.4**).

When the XRD graph is examined, the peaks of cristobalite were detected around 22° and 31°, similar to the samples sintered at 1450°C and 1500°C.

While the peaks of mullite, zircon, and cristobalite can be identified in the structure, the peaks of iron-oxide could not be detected, as in the XRD analysis performed at 1450°C and 1500°C due to the low weight % additive and the overlap of the XRD peaks of iron oxide in the mullite-zircon system.

No evidence was found for the new phase formation from the X-Ray diffraction peaks of samples with iron-oxide sintering aid addition at the sintering temperature of 1450°C.

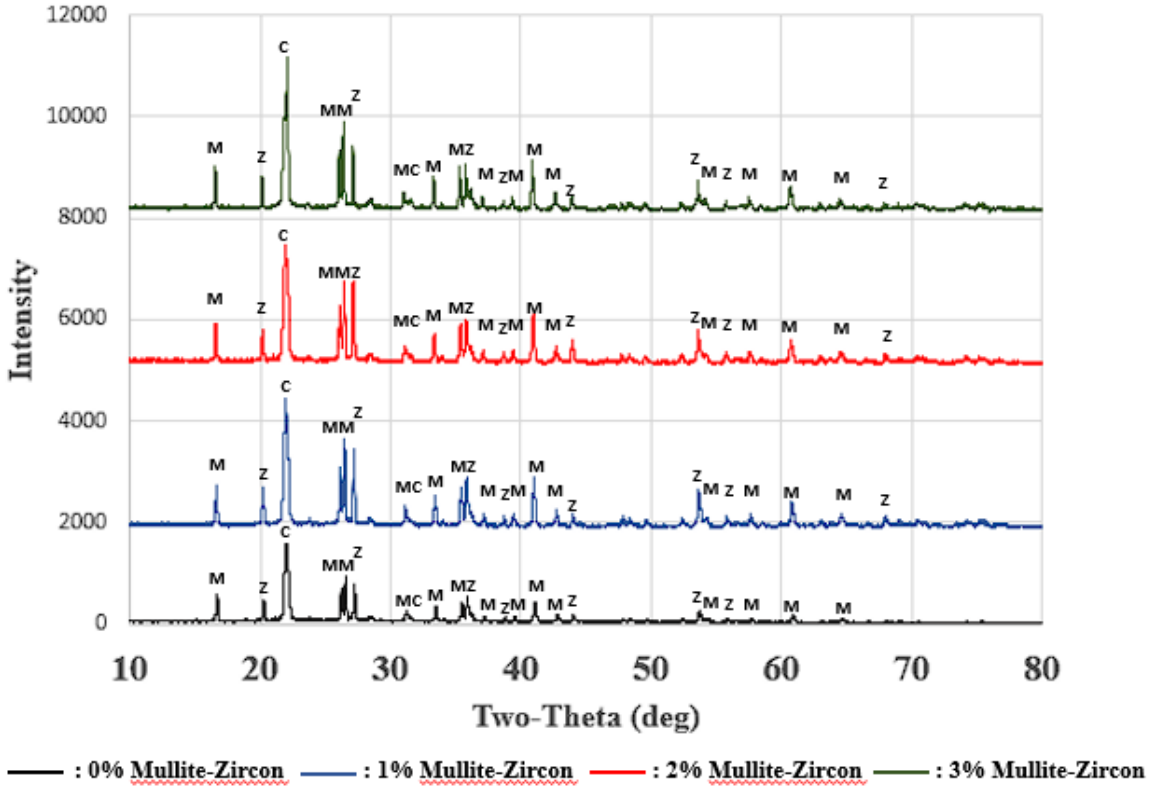


Figure 4.4 XRD graph of Mullite-Zircon structure sintered at 1400°C with the addition of Iron-Oxide 0%,1%,2%, and 3% respectively. Mullite (M), Zircon (Z), Cristobalite (C).

The change of the mullite-zircon structure without iron-oxide addition on the phases with temperature was investigated using the X-Ray Diffraction method.

As stated in the section examining the XRD peaks at 1550°C, it is clear that the peaks of the cristobalite phase found in the samples sintered at 1400°C, 1450°C, and 1500 °C, are not found in the samples sintered at 1550°C due to glassy phase formation.

In addition, the effect of temperature change on X-Ray Diffraction peaks caused

peak shifts. A slight shift was observed in the XRD peaks and the intensity values (**Figure 4.5**).

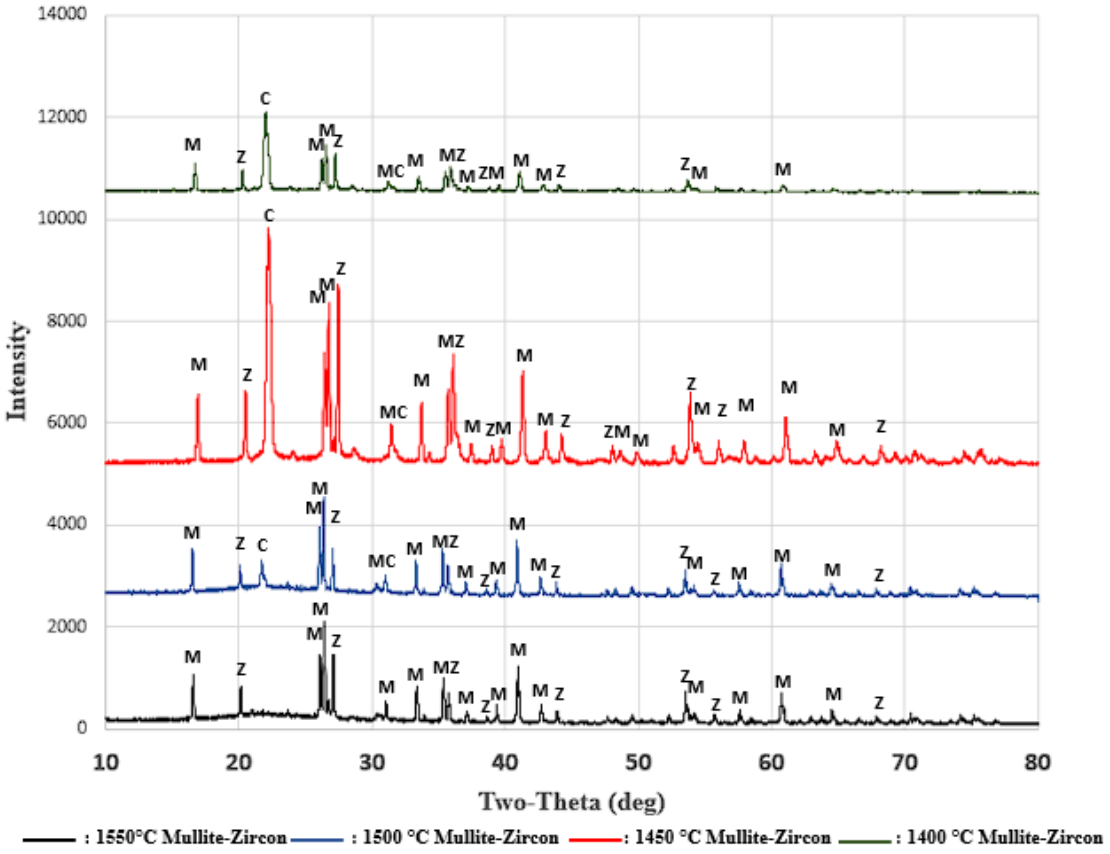


Figure 4.5 XRD graph of Mullite-Zircon structure sintered at the temperature of 1550°C, 1500°C, 1450°C, and 1400°C respectively. Mullite (M), Zircon (Z), Cristobalite (C).

4.2. Density

5. Bulk density measurements made according to the Archimedes principle for each temperature and each additive were taken over 3 samples and the average value was calculated using the bulk density formula **(3.3)**. The results are given in the graph below (**Figure 4.6**).

When the iron-oxide-free samples are examined and error bars are taken into account, the highest value in bulk density occurred in the sample sintered at 1550°C and the lowest value was observed at 1400 °C.

It has been observed from the bulk density graph (**Figure 4.6**) that the additive contributes positively to the density for 1% and 2% at 1450°C, but 3% additive reduces the density. A slight negative effect of the 1500°C additive on the density was observed.

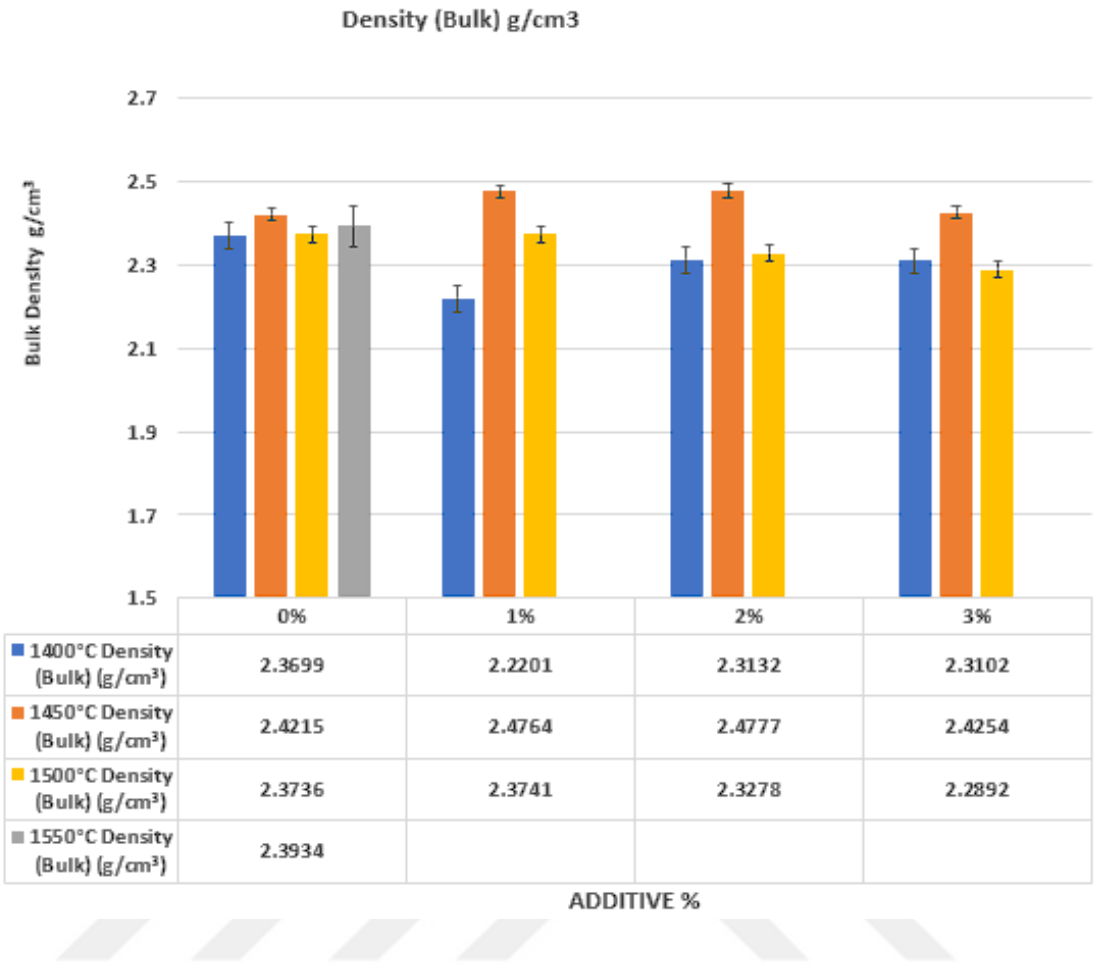


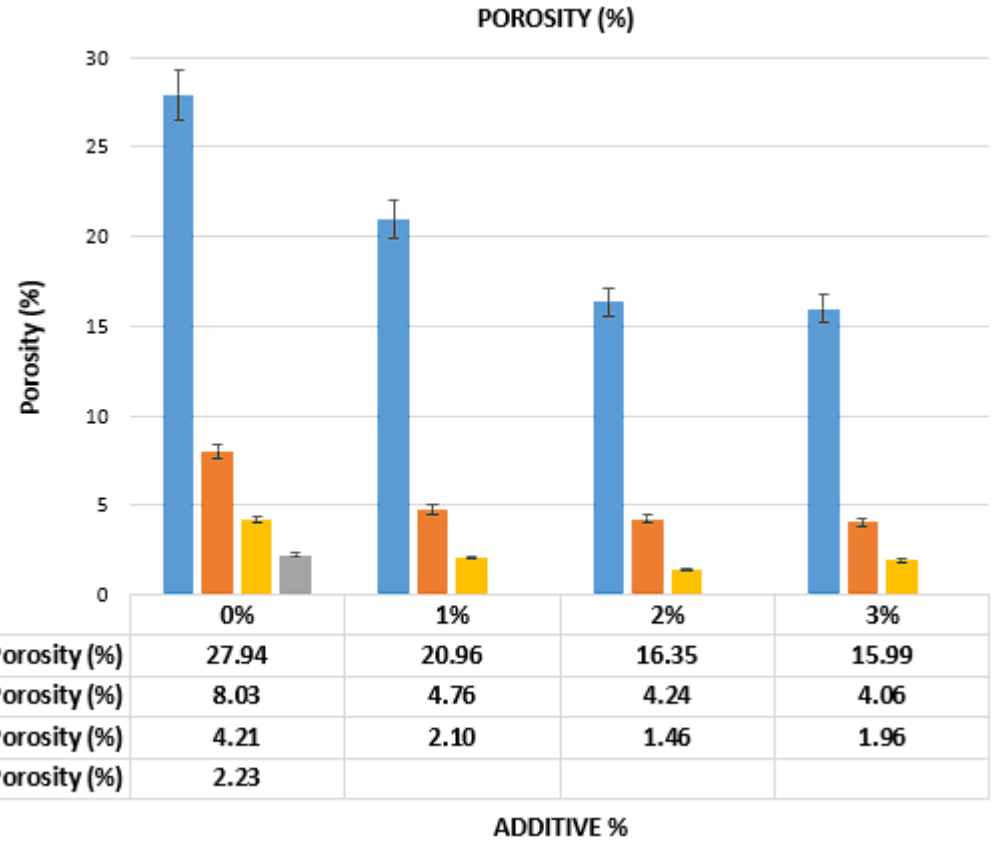
Figure 4.6 Bulk density g/cm^3 – Additive % graph.

Since errors may occur in the measurements due to surface cracks and part breakage that occur after sintering, it has been observed that there is not a significant difference when the results are examined in standard deviations.

4.3. Porosity

The data obtained in the experiment performed according to the Archimedes principle were used to determine the % porosity of the samples. At each temperature and each additive percentage was taken into consideration, measurements were made on 3 samples and the average was calculated. The formulas given in (**3.3**) were used in the calculations.

The effect of sintering aid additive on % porosity was investigated. The data obtained were shown for each temperature in the Porosity (%) – Additive (%) graph and the values were given in the table below graph. (**Figure 4.7**).



	0%	1%	2%	3%
1400°C Porosity (%)	27.94	20.96	16.35	15.99
1450°C Porosity (%)	8.03	4.76	4.24	4.06
1500°C Porosity (%)	4.21	2.10	1.46	1.96
1550°C Porosity (%)	2.23			

Figure 4.7 Porosity (%) - Additive (%) graph.

According to the results obtained, the samples sintered at 1400°C give the highest porosity value at every temperature and with % sintering aid additive. The effect of the sintering aid addition to mullite-zircon mixture on reducing the porosity was evaluated for the samples sintered at all chosen sintering temperatures.

The porosity of the samples sintered at 1450°C was significantly reduced compared to samples sintered at 1400°C. This decrease appears to be due to the effect of temperature.

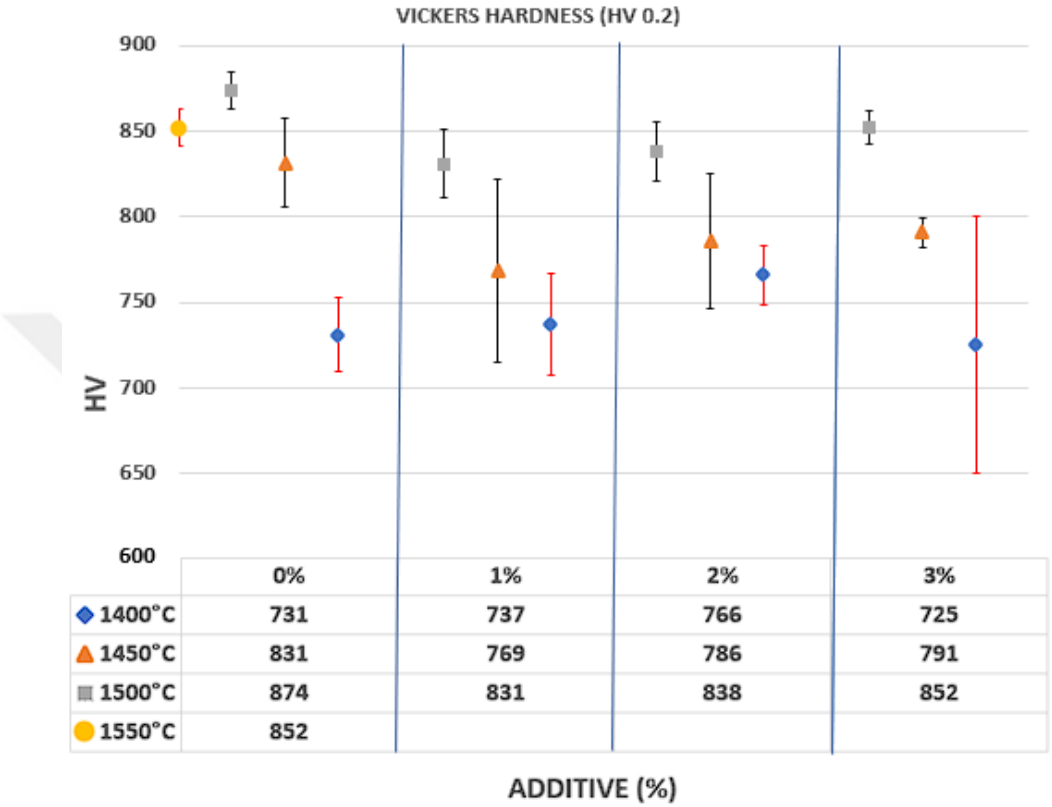
The porosity value, which was 24.94% for mullite-zircon without additives at 1400°C, decreased to 8.02% as the temperature increased to 1450°C. At the same time, it was observed that the porosity value was reduced due to the increase in the percentage of additive material at 1450°C. At this temperature, the lowest porosity value was found to be 4.06% in the samples with 3% sintering aid addition.

For the samples sintered at 1500°C, a decrease in the porosity was observed with the increase in temperature and the addition of the sintering aid into the mullite-zircon mixture. Mullite-zircon structure with 2% sintering aid addition gives the lowest porosity value of 1.45%.

It was observed that the porosity value was also reduced in the samples sintered at 1500°C and with an addition of 1 wt.%, 2 wt.%, and 3 wt.% compared to the test samples sintered at 1550°C without additives.

4.4. Hardness

The Vickers hardness measurement was performed, and 3 indents from each sample with different sintering temperatures and sintering aid (Fe_2O_3) addition were taken under a load of 200 grams. The average hardness values and comparison were given in the graph (**Figure 4.8**).



	0%	1%	2%	3%
1400°C	731	737	766	725
1450°C	831	769	786	791
1500°C	874	831	838	852
1550°C	852			

Figure 4.8 Vickers Hardness (HV) – Additive % graph.

Considering the values given in (**Figure 4.8)**, a decrease in material hardness is observed at 1400°C. At 1400°C, the highest hardness value was found 766 HV in samples containing 2% sintering aid additive, and the lowest value was found 725 HV with 3% sintering aid addition. When the error function is taken into account, the hardness values of 0%, 1%, and 3% are relatively close.

The highest hardness value of 874 HV was found on the mullite-zircon structure without additive sintered at 1500°C.

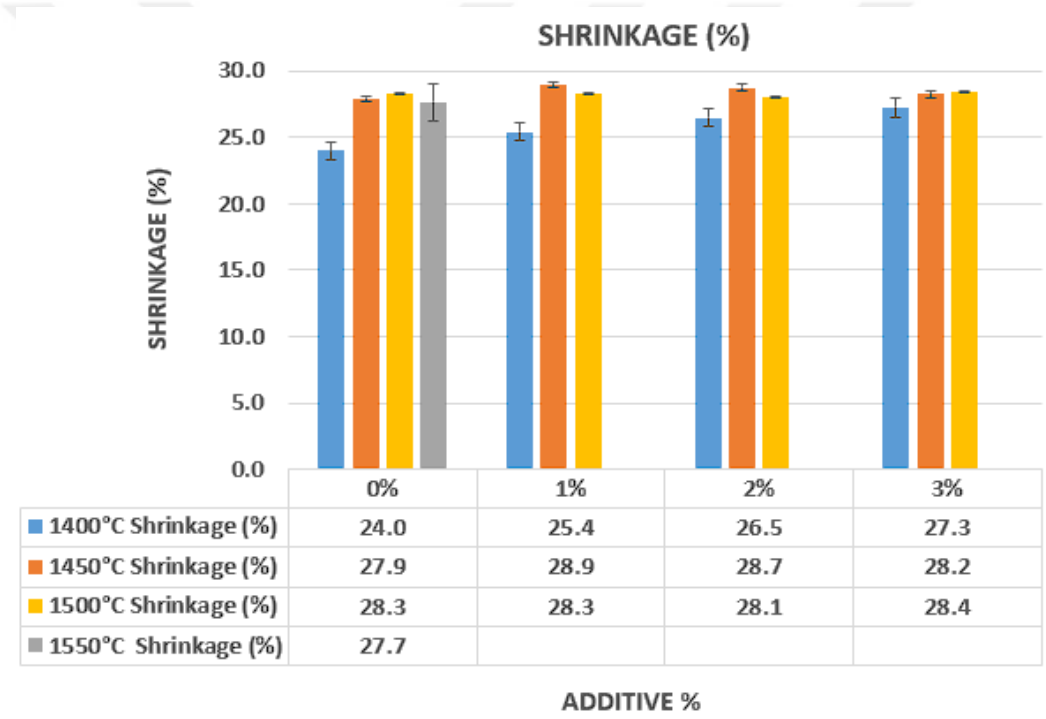
A decrease in the hardness value was observed with the addition of 1 wt.% Fe_2O_3 in the samples sintered at 1450°C and 1500°C. However, the hardness value of the samples linearly increased with the addition of 2 wt.% and 3 wt.% respectively.

In this study, the highest hardness value of 874 HV was found in mullite zircon without sintering aid addition, while the lowest hardness value of 725HV was found in samples sintered at 1400°C with 3 wt.% Fe_2O_3 addition.

The hardness decreased slightly with the addition of iron oxide, but an increase in the hardness values was observed with the addition of 2% and 3% iron oxide, as the porosity decreased.

4.5. Surface Area Shrinkage

Surface area shrinkage (%) values were calculated by using the equation of (**3.4**) for the samples sintered at each sintering temperature and Fe_2O_3 wt.% addition. The increase in sintering temperature plays an important role in the shrinkage of sintered samples.



	0%	1%	2%	3%
1400°C Shrinkage (%)	24.0	25.4	26.5	27.3
1450°C Shrinkage (%)	27.9	28.9	28.7	28.2
1500°C Shrinkage (%)	28.3	28.3	28.1	28.4
1550°C Shrinkage (%)	27.7			

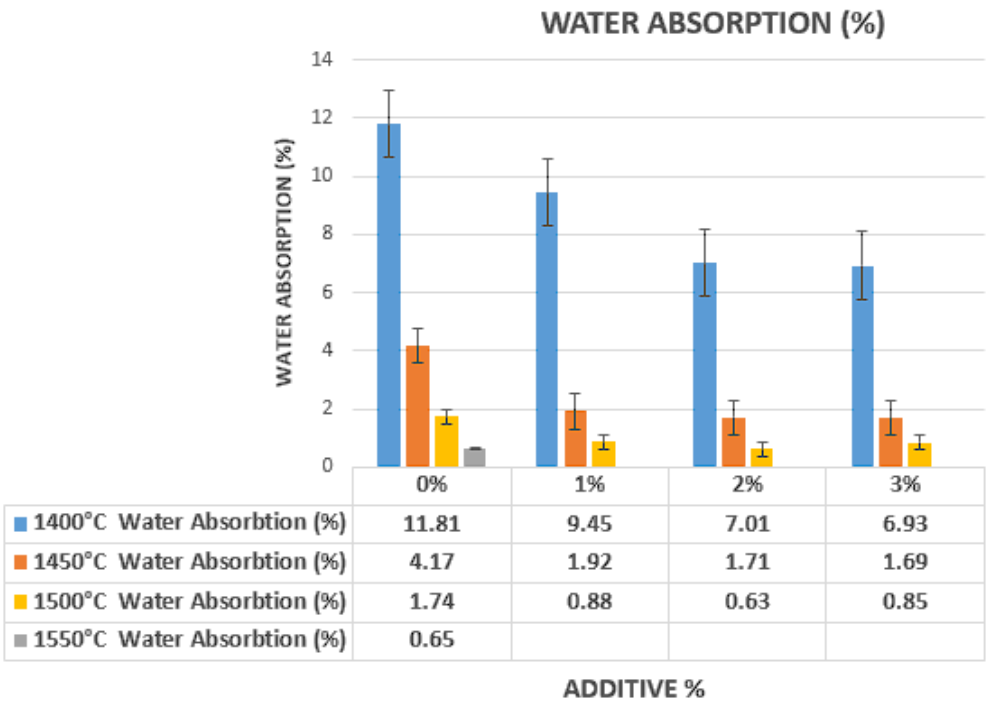
Figure 4.9 Shrinkage (%) - Additive (%) graph.

Sintering at the temperature of 1400°C, the increase in shrinkage (%) with the addition of additives is more apparent than in the samples sintered at higher temperatures (**Figure 4.9**).

Considering the error bars in the samples without additives, the highest shrinkage (%) value was observed at 1550°C, as expected. When the mullite-zircon mixture with Fe_2O_3 addition at 1450°C and 1500°C were examined, it was observed that the additive did not cause a significant change in the shrinkage of the material. The factor that makes the important change here is the sintering temperature.

4.6. Water Absorption

Water absorption analysis was applied for the samples with sintering auxiliary additive at different temperatures and different wt.% (**Figure 4.10**). In this study, the average of the calculations made on 3 samples for each temperature and wt.% additive is given. The results for the samples sintered at different temperatures and wt.% addition is given in the graph below.



	0%	1%	2%	3%
1400°C Water Absorbtion (%)	11.81	9.45	7.01	6.93
1450°C Water Absorbtion (%)	4.17	1.92	1.71	1.69
1500°C Water Absorbtion (%)	1.74	0.88	0.63	0.85
1550°C Water Absorbtion (%)	0.65			

Figure 4.10 Water absorption (%) - Additive (%) graph.

In this graph (**Figure 4.10**), it was determined that the water absorption % reaches its highest value at 0 wt.% at 1400°C. It was observed that the water absorption % decreased with the addition of a sintering aid additive. It was determined that the lowest value of water absorption value for 1400°C was 3 wt.% Fe_2O_3 added mullite-zircon mixture.

For the samples sintered at 1450°C with different additives, a significant decrease in water absorption % was observed compared to the samples sintered at 1400°C. At the temperature of 1400°C, it was observed that the % water absorption value decreased when the weight percentage of the additive increased at 1450°C.

It was found that the percentage of water absorption in samples sintered at 1500°C, depending on the sintering temperature, from samples sintered at 1450°C was low for each additive percentage. The lowest measured water absorption value among the samples was 0.63% with 2 wt.% Fe_2O_3 addition. Considering these error bars in the graph, the samples containing additives and sintered at 1500°C, almost the same values were determined.

However, when observing the sample without sintering aid addition and sintered at 1500°C, it is seen that the sintering aid additive reduces the water absorption (%).

When compared to the test sample without additives sintered at 1550°C, it was determined that the water absorption percentage increased with the decrease of the sintering temperature, and when the additive was added, the water absorption percentage approached the test sample with the addition of additives to sintering at 1500°C. In addition, the sintering aid additive plays a significant role in reducing the water absorption percentage in the mullite-zircon mixture for each sintering temperature.

In this study, the highest water absorption of 11.81% was found when the sample sintered at the temperature of 1400°C without sintering aid addition to the mullite-zircon mixture, and the lowest water absorption of 0.63% was found when the sample sintered at the temperature of 1500°C with 2 wt.% sintering aid (Fe_2O_3) addition to the mullite-zircon mixture.

4.7. Microstructure Evaluation

Mullite-Zircon mixtures are sintered at elevated temperatures (above 1500 °C) to improve density and for required mechanical properties. In this study, Fe_2O_3 particles were used as sintering promoters or to promote liquid phase sintering to reduce the sintering temperature and improve the density of the Mullite-Zircon mixtures.

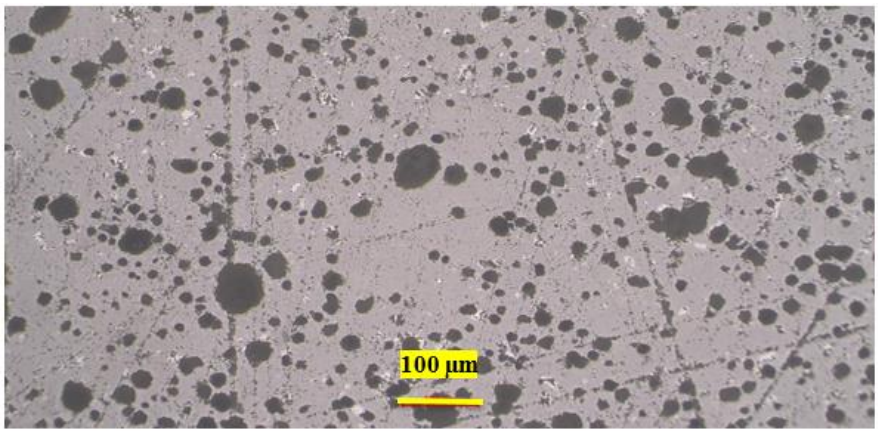


Figure 4.11 1550°C sintered mullite-zircon microstructure without iron-oxide addition with magnification 50x.

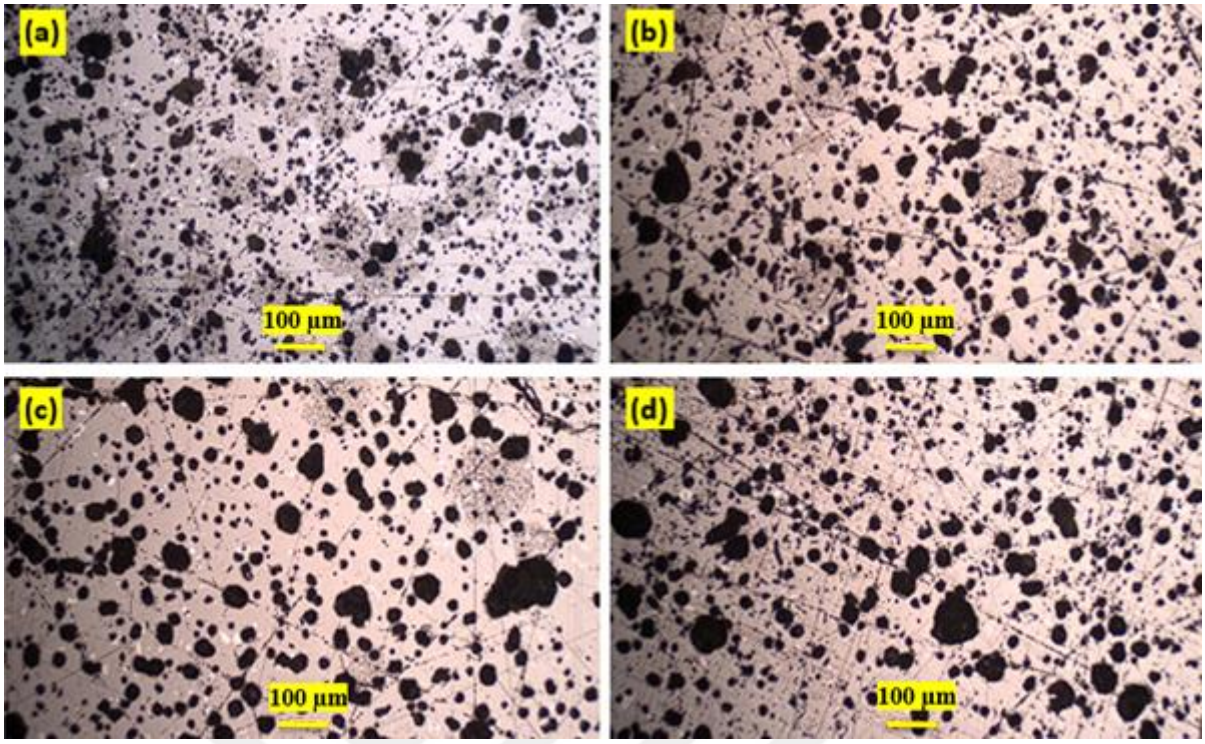


Figure 4.12 1500°C sintered mullite-zircon microstructure with iron-oxide addition (a) 0 wt.%, (b) 1 wt.% (c) 2 wt.% (d) 3 wt.%, with magnification 50x.

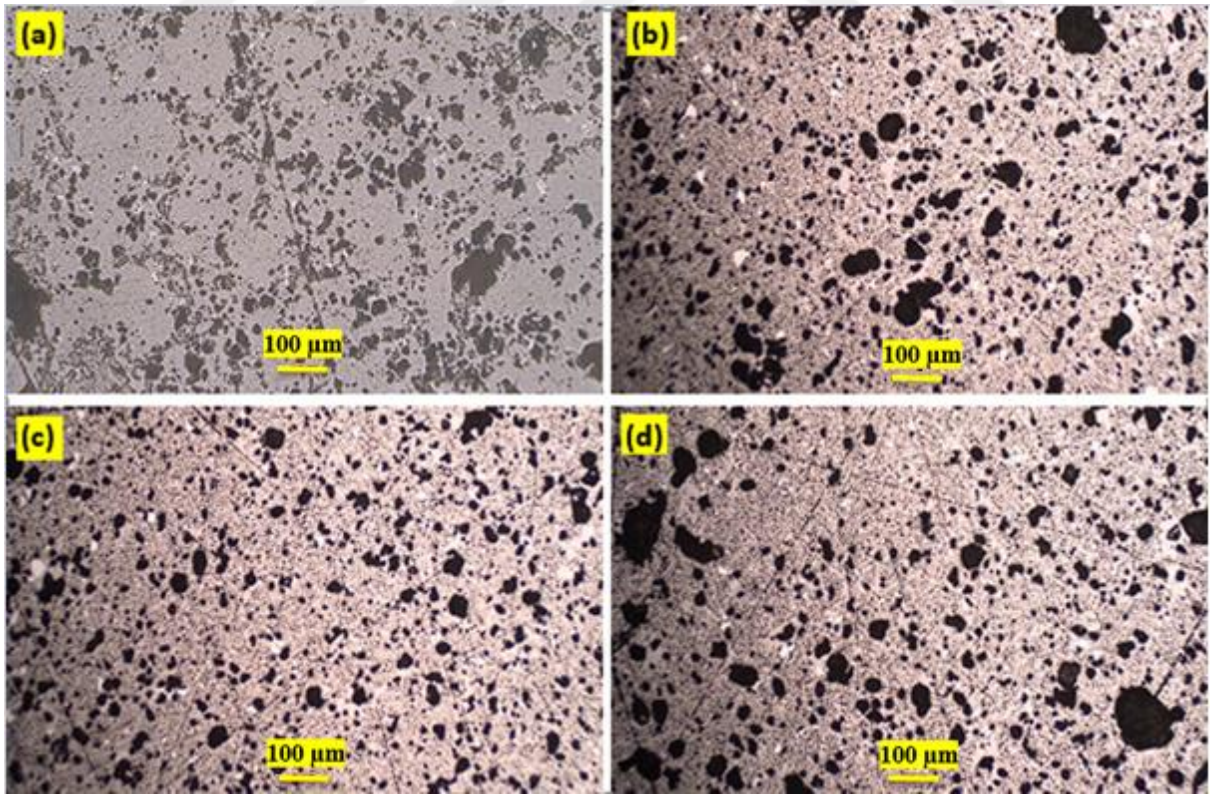


Figure 4.13 1450°C sintered mullite-zircon microstructure with iron-oxide addition (a) 0 wt.%, (b) 1 wt.% (c) 2 wt.% (d) 3 wt.%, with magnification 50x.

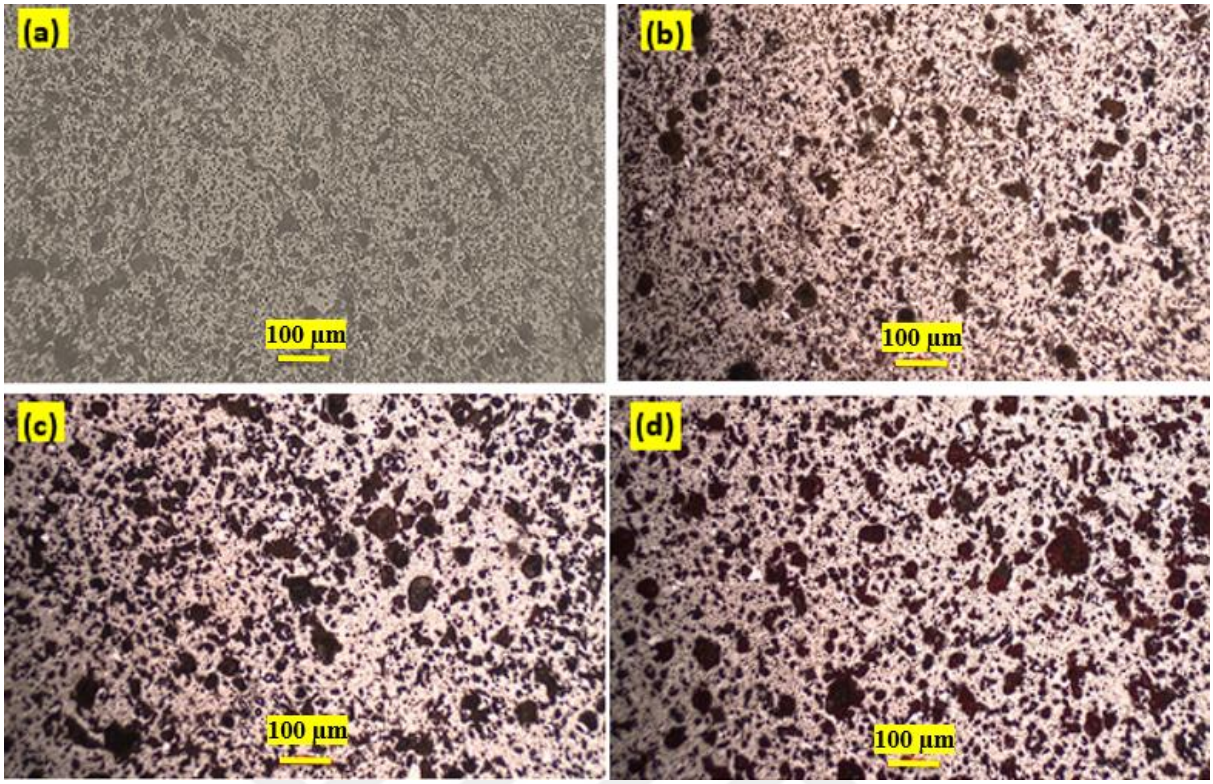


Figure 4.14 1400°C sintered mullite-zircon microstructure with iron-oxide addition (a) 0 wt.%, (b) 1 wt.% (c) 2 wt.% (d) 3 wt.%, with magnification 50x.

Microstructure images with and without sintering aid addition were given for the sintering temperatures of 1550°C, 1500°C, 1450°C and 1400°C in the figures above (**Figure 4.11-4.14**).

Generally, it was observed that as the temperature increases the porosity decreases, and the densification is improved. No clear reaction products or bonding was identified and a phase formed between iron and oxide and the Mullite –Zircon mixture.

5. CONCLUSIONS

i) It has been observed that the cristobalite phase, which is present in the structure at 1400°C, 1450°C, and 1500°C may have turned into a glassy phase when the sintering temperature was increased to 1550°C. Mullite-zircon peaks could be observed from the XRD graph. No different or new phase formation was detected with the iron-oxide addition.

ii) Sintering aid additive iron-oxide provides the best positive effect on the density for the addition of 1 wt.%- 2 wt.% at 1450°C, but higher addition may have a negative effect on the mullite-zircon mixture.

iii) It was observed that the porosity value was reduced in the samples sintered at 1500°C and with an addition of 1 wt.%, 2 wt.%, and 3 wt.% compared to the test samples sintered at 1550°C without additives. Iron-oxide addition and an increase in the sintering temperature have a positive effect on reducing porosity.

iv) An increase in the hardness values was observed with the addition of 2 wt.% and 3 wt.% iron-oxide for the temperature of 1450°C and 1500°C. 1 wt.% iron-oxide addition to the sample has a negative effect on the hardness of the material.

v) The iron-oxide addition did not cause a significant change in the shrinkage of the material. An increase in sintering temperature slightly increases the shrinkage.

vi) The lowest water absorption value of 0.63% was found when the sample sintered at the temperature of 1500°C with 2 wt.% iron-oxide addition. Water absorption value decreases when both iron-oxide addition and sintering temperature rises.

vii) The optical microstructural evaluation was performed by using two different parameters first by temperature effect and secondly by the addition of hematite. It was found that increase in sintering temperature and sintering aid addition into Mullite-Zircon mixture promoting sintering and reducing porosity. These results suggest that they have a positive effect on the densification of the microstructure.

6. REFERENCES

[1] W. Barsoum, Fundamentals of Ceramics, London: Institute of Physics Publishing, 2003, pp. 2, 8.

[2] W. D. Kingery, H. K. Bowen and D. R. Uhlmann, Introduction to Ceramics, New York: John-Wiley and Sons Inc., 1976, pp. 1, 304-307.

[3] R. B. Heimann, Classic and Advanced Ceramics: From Fundamentals to Applications, Weinheim: WILEY-VCH Verlag GmbH Co., 2010, p. 1.

[4] G. C. Philips, A Concise Introduction to Ceramics, New York: Van Nostrand Reinhold, 1991, p. 3.

[5] K. K. Chawla, Ceramic Matrix Composites: Second Edition, New York: Springer Science+Business Media, 2003, pp. 1-2.

[6] I. M. Low, Advances in Ceramic Matrix Composites, Cambridge: Woodhead Publishing Limited, 2014, p. 1.

[7] C. B. Carter and M. G. Norton, Ceramic Materials: Science and Engineering, New York: Springer-Verlag, 2003, p. 111.

[8] J. -J. Shyu and Y. -C. Chen, "Zirconia-mullite ceramics made from composite particles coated with amorphous phase: I. Effect of zirconia addition," *Journal of Materials Research*, vol. 10, no. 1, pp. 63-70, 1995.

[9] E. R. Rangel, S. D. De La Torre, M. Umemoto, H. Miyamoto and H. Balmori-Ramirez, "Zirconia-Mullite Composites Consolidated by Spark Plasma Reaction Sinterind from Zircon and Alumina," *Journal of the American Ceramic Society*, vol. 88, no. 5, pp. 1150-1157, 2005.

[10] J. F. Shackelford and R. H. Doremus, Ceramic and Glass Materials: Structure, Properties and Processing, New York: Springer Science+Business Media, 2008, pp. 32-33.

[11] H. Schneider, J. Schreuer and B. Hildmann, "Structure and properties of mullite - A review," *Journal of the European Ceramic Society*, vol. 28, pp. 329-344, 2008.

[12] Y. Shi, X. Huang and D. Yan, "Fabrication of hot-pressed zircon ceramics: mechanical properties and microstructure," *Ceramics International*, vol. 23, pp. 457-462, 1997.

[13] A. Kaiser, M. Lobert and R. Telle, "Thermal stability of zircon (ZrSiO4)," *Journal of the European Ceramic Society*, vol. 28, pp. 2199-2211, 2008.

[14] R. C. Selley, I. R. Plimer, L. R. M. Cocks and J. McCall, Encyclopedia of Geology, Oxford: Elsevier Academic Press, 2005, p. 601.

[15] F. L. Pirkle and D. A. Podmeyer, Zircon: Origin and Uses, vol. 292, Society for Mining, Metallurgy, and Exploration, Inc., 1993.

[16] R. Telle, F. Greffrath and R. Prieler, "Direct observation of the liquid miscibility gap in the zirconia–silica system," *Journal of the European Ceramic Society,* vol. 35, pp. 3995-4004, 2015.

[17] N. M. Rendtorff, L. B. Garrido and E. F. Aglietti, "Mechanical and fracture properties of zircon–mullite composites obtained by direct sintering," *Ceramics International,* vol. 35, pp. 2907-2913, 2009.

[18] M. S. Baspinar and F. Kara, "Optimization of the Corrosion Behavior of Mullite Refractories against Alkali Vapor Vvia ZrSiO4 Addition to the Binder Phase," *Ceramics Silikaty,* vol. 53, no. 4, pp. 242-249, 2009.

[19] S.-J. L.Kang, Sintering, Burlington: Elsevier, 2005.

[20] R. De Oro calderon, C. Gierl-Mayer and H. Danninger, "Fundamentals of Sintering: Liquid Phase Sintering," in *Reference Module in Materials Science and Materials Engineering*, Elsevier, 2021.

[21] H. Aydın, "Bor mineralleri katkılı müllit/zirkonya kompozit üretimi (The synthesis of mullite/zirconia composite materials doped with boron minerals)," PhD Thesis, Dumlupınar University, Kütahya, 2013.

[22] K. Das, B. Mukherjee and G. Banerjee, "Effect of Yttria on Mechanical and Microstructural Properties of Reaction Sintered Mullite-Zirconia Composites," *Journal of the European Ceramic Society,* vol. 18, pp. 1771-1777, 1998.

[23] F. Ren, Z. Wang, Z. Ma, J. Su, F. Li and L. Wang, "Effects of Fe2O3 concentration on microstructures and properties of SiC-based ceramic foams," *Materials Science and Engineering A,* pp. 113-116, 2009.

[24] A. Mehranjani, D. J. Cumming, D. C. Sinclair and R. H. Rothman, "Low-temperature co-sintering for fabrication of zirconia/ceria bi-layer electrolyte via tape casting using a Fe2O3 sintering aid," *Journal of the European Ceramic Society,* vol. 37, pp. 3981-3993, 2017.

[25] W. D. Callister and D. G. Rethwisch, Material Science and Engineering an Introduction, 9 ed., Wiley, 2014, pp. 88-89.

[26] W. D. Callister and D. G. Rethwisch, Material Science and Engineering, 8 ed., Wiley, 2010, pp. 174-179.

[27] *ASTM C373-18, Standard Test Methods for Determination of Water Absorption and Associated Properties by Vacuum Method for Pressed Ceramic Tiles and Glass Tiles and Boil Method for Extruded Ceramic Tiles and Non-tile Fired Ceramic Whiteware Products,* Feb 13, 2018.

BIOGRAPHY

Elif Bal, Following her high school graduation from Istanbul Anadolu Lisesi in 2012, she attended Gebze Technical University, Department of Material Science and Engineering. After completing her degree in 2017, she did earn tuition at Marmara University, Department of Metallurgy and Materials Engineering for her MSc. studies in 2019.